Chapter 3
Crystals

La science cristallographique ne consiste donc point à décrire scrupuleusement tous les accidens des formes cristallines; mais à spécifier, en décrivant ces formes, les rapports plus ou moins immédiats qu'elles ont entre elles.
Crystallographic science does not consist in the scrupulous description of all the accidents of crystalline form, but in specifying, by the description of these forms, the more or less close relationship they have with each other.
J.-B. Romé de l'Isle, 1783 [165]

Abstract A little bit of crystallography… The concepts of the direct and reciprocal lattice, point and space groups, unit and elementary cells and the Wigner–Seitz cell are laid out. The important crystal structures for semiconductors (diamond, sphalerite, wurtzite, chalcopyrite,…) are discussed in some detail. Also alloys and ordering are covered.

3.1 Introduction

The economically most important semiconductors have a relatively simple atomic arrangement and are highly symmetric. The symmetry of the atomic arrangement is the basis for the classification of the various crystal structures. Using group theory [166], basic and important conclusions can be drawn about the physical properties of the crystal, such as its elastic and electronic properties. The presence of highly symmetric planes is obvious from the crystal shape of the minerals and their cleavage behavior.

Polycrystalline semiconductors consist of grains of finite size that are structurally perfect but have various orientations. The grain boundaries are a lattice defect (see also Sect. 4.4.3). Amorphous semiconductors are disordered on the atomic scale, see Sect. 3.3.7.

M. Grundmann, *The Physics of Semiconductors*, Graduate Texts in Physics,
DOI 10.1007/978-3-319-23880-7_3

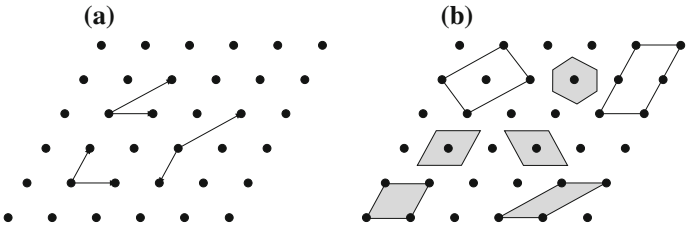

Fig. 3.1 (**a**) Two-dimensional lattice. It can be generated by various pairs of translation vectors. (**b**) Elementary cells of the lattice. Primitive elementary cells are *shaded*

3.2 Crystal Structure

A crystal is built up by the (quasi-) infinite periodic repetition of identical building blocks. This lattice (Bravais lattice) is generated by the three fundamental *translation* vectors $\mathbf{a}_1$, $\mathbf{a}_2$ and $\mathbf{a}_3$. These three vectors may not lie in a common plane. The lattice (Fig. 3.1) is the set of all points $\mathbf{R}$

$$\mathbf{R} = n_1\,\mathbf{a}_1 + n_2\,\mathbf{a}_2 + n_3\,\mathbf{a}_3. \tag{3.1}$$

The crystal structure is made up by the lattice and the building block that is attached to each lattice point. This building block is called the *base* (Fig. 3.2). In the simplest case, e.g., for crystals like Cu, Fe or Al, this is just a single atom (monoatomic base). In the case of C (diamond), Si or Ge, it is a diatomic base with two identical atoms (e.g., Si–Si or Ge–Ge), in the case of compound semiconductors, such as GaAs or InP, it is a diatomic base with nonidentical atoms such as Ga–As or In–P. There exist far more involved structures, e.g., $NaCd_2$ where the smallest cubic cell contains 1192 atoms. In protein crystals, the base of the lattice can contain 10 000 atoms.

In summary: Crystal structure = Lattice × Base.

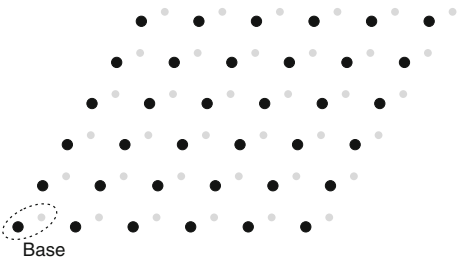

Fig. 3.2 Crystal structure, consisting of a lattice and a base

3.3 Lattice

As described in Sect. 3.2 the lattice is spanned by three vectors $\mathbf{a}_i$. The lattice symmetry is decisive for the physical properties of the semiconductor. It is described by the appropriate groups of the symmetry operations.

3.3.1 Unit Cell

The choice of the vectors $\mathbf{a}_i$ making up the lattice is not unique (Fig. 3.1). The volume that is enclosed in the parallelepiped spanned by the vectors $\mathbf{a}_1$, $\mathbf{a}_2$ and $\mathbf{a}_3$ is called the *elementary cell*. A *primitive* elementary cell is an elementary cell with the smallest possible volume (Fig. 3.1b). In each primitive elementary cell there is exactly *one* lattice point. The coordination number is the number of next-neighbor lattice points. A primitive cubic (pc) lattice, e.g., has a coordination number of 6.

The typically chosen primitive elementary cell is the *Wigner–Seitz* (WS) cell that reflects the symmetry of the lattice best. The Wigner–Seitz cell around a lattice point $\mathbf{R}_0$ contains all points that are closer to this lattice point than to any other lattice point. Since all points fulfill such a condition for some lattice point $\mathbf{R}_i$, the Wigner–Seitz cells fill the volume completely. The boundary of the Wigner–Seitz cell is made up by points that have the same distance to $\mathbf{R}_0$ and some other lattice point(s). The Wigner–Seitz cell around $\mathbf{R}_0$ is constructed by drawing lines from $\mathbf{R}_0$ to the next neighbors $\mathbf{R}_j$, taking the point at half distance and erecting a perpendicular plane at $(\mathbf{R}_j + \mathbf{R}_0)/2$. The WS cell is the smallest polyhedra circumscribed by these planes. A two-dimensional construction is shown in Fig. 3.3.

3.3.2 Point Group

Besides the translation there are other operations under which the lattice is invariant, i.e. the lattice is imaged into itself. These are:

Identity. The neutral element of any point group is the identity that does not change the crystal. It is denoted as 1 (E) in international (Schönfließ) notation.

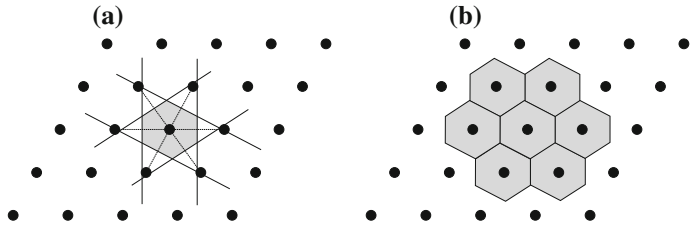

Fig. 3.3 (**a**) Construction of a two-dimensional Wigner–Seitz cell, (**b**) filling of space with WS cells

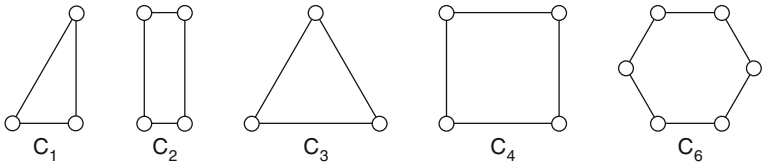

Fig. 3.4 Two-dimensional objects with perpendicular rotation axis C_n. Note that the *circles* do not exhibit σ_h symmetry with respect to the paper plane, i.e. they are different on the *top* and *bottom side*

Rotation. The rotation around an axis may have a rotation angle of 2π, $2\pi/2$, $2\pi/3$, $2\pi/4$ or $2\pi/6$ or their integer multiples. The axis is then called n = 1-, 2-, 3-, 4- or 6-fold, respectively,[1] and denoted as n (international notation) or C_n (Schönfließ). Objects with C_n symmetry are depicted in Fig. 3.4.

Mirror operation with respect to a plane through a lattice point. Different mirror planes are discerned (Fig. 3.5) (after Schönfließ) σ_h: a mirror plane perpendicular to a rotational axis, σ_v: a mirror plane that contains a rotational axis, and σ_d: a mirror plane that contains a rotational axis and bisects the angle between two C_2 axes. The international notation is $\bar{2}$.

Inversion. All points around the inversion center $\mathbf{r}$ are replaced by $-\mathbf{r}$. The inversion is denoted $\bar{1}$ (i) in international (Schönfließ) notation.

Improper rotation. The improper rotation S_n is a rotation C_n followed immediately by the inversion operation i denoted as $\bar{n}$ in international notation. There are $\bar{3}$, $\bar{4}$ and $\bar{6}$ and their powers. Only the combined operation $\bar{n}$ is a symmetry operation, while the individual operations C_n and i alone are not symmetry operations. In the Schönfließ notation the improper rotation is defined as $S_n = \sigma_\mathrm{h} C_n$, with σ_h being a mirror operation with a plane perpendicular to the axis of the C_n rotation, denoted as S_n. There are S_3, S_4 and S_6 and $\bar{3} = S_6^5$, $\bar{4} = S_4^3$ and $\bar{6} = S_3^5$. For successive applications, the S_n yield previously known operations, e.g., $S_4^2 = C_2$, $S_4^4 = E$, $S_6^2 = C_3$, $S_6^3 = i$, $S_3^2 = C_3^2$, $S_3^3 = \sigma_\mathrm{h}$, $S_3^4 = C_3$, $S_3^6 = E$. We note that formally S_1 is the inversion i and S_2 is the mirror symmetry σ. Objects with S_n symmetry are schematically shown in Fig. 3.6.

These symmetry operations form 32 *point groups*. These groups are shown (with their different notations and elements) in Table B.2. The highest symmetry is the cubic symmetry $O_h = O \times i$. The tetraeder group T_d (methane molecule) is a subgroup of O_h, lacking the inversion operation.

Important for surface symmetries, there are ten two-dimensional point groups (Sect. 11.2 and Table B.1).

[1] 5-fold periodic symmetry is geometrically impossible. However, *quasicrystals* with aperiodic five-fold symmetry exist [167, 168], some of them possibly being semiconducting [169, 170].

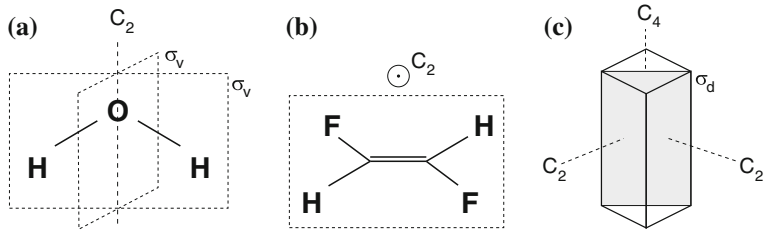

Fig. 3.5 Mirror planes: (**a**) σ_v (at H_2O molecule), (**b**) σ_h (at F_2H_2 molecule) and (**c**) σ_d

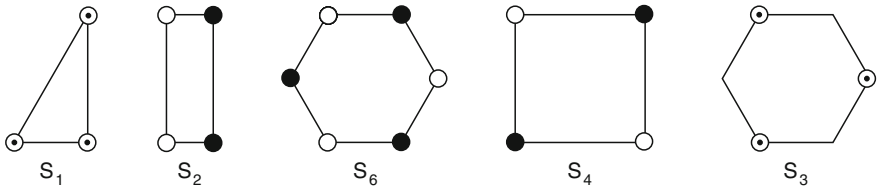

Fig. 3.6 Two-dimensional objects with perpendicular improper rotation axis S_n. Note that the *white* and *black circles* do not exhibit σ_h symmetry with respect to the paper plane, i.e. they are *white on the top* and *black on the bottom*. The *circles with a dot in the center* exhibit σ_h symmetry, i.e. they look the same from *top* and *bottom*

3.3.3 Space Group

The space group is formed by the combination of the elements of the point group with translations. The combination of a translation along a rotational axis with a rotation around this axis creates a screw axis n_m. In Fig. 3.7a, a so-called 4_1 screw axis is shown. The first index n indicates the rotation angle, i.e. $2\pi/n$, the second index indicates the translation, i.e. $c\,m/n$, c being the periodicity along the axis. There are eleven crystallographically allowed screw rotations.[2]

The combination of the mirror operation at a plane that contains a rotational axis with a translation along this axis creates a glide reflection (Fig. 3.7b). For an axial glide (or b-glide) the translation is parallel to the reflection plane. A diagonal glide (or d-glide) involves translation in two or three directions. A third type of glide is the diamond glide (or d-glide). There are 230 different space groups, listed in Appendix B. A detailed treatment can be found in [171].[3]

Important for surface symmetries, there are 17 two-dimensional space groups (Sect. 11.2).

[2] $2_1, 3_1, 3_2, 4_1, 4_2, 4_3, 6_1, 6_2, 6_3, 6_4, 6_5$.

[3] One should in particular consider the pitfalls pointed out in Appendix 10 of this reference.

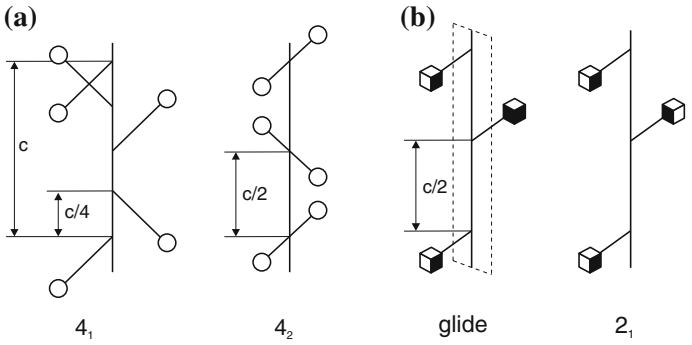

Fig. 3.7 (**a**) Schematic drawing of a 4_1 and 4_2 screw axis. (**b**) Schematic drawing of an axial glide reflection. The mirror plane is shown with *dashed outline*. Opposite faces of the cube have opposite color. For comparison a 2_1 screw axis is shown

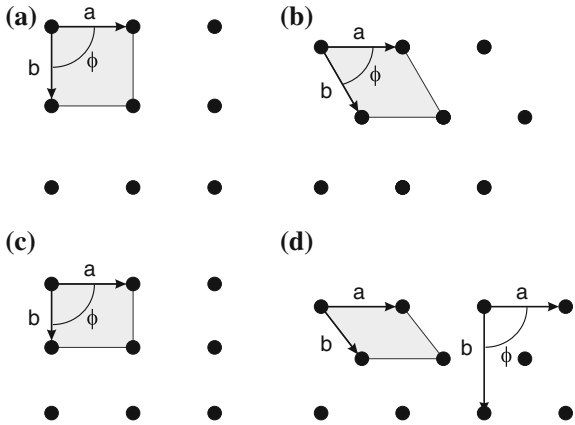

Fig. 3.8 The two-dimensional Bravais lattices with the primitive unit cells: (**a**) *square lattice* ($a = b$, $\phi = 90°$), (**b**) *hexagonal lattice* ($a = b$, $\phi = 60°$), (**c**) *rectangular lattice* ($a \neq b$, $\phi = 90°$), (**d**) *centered-rectangular lattice* ($a \neq b$, $\phi = 90°$, for the (nonprimitive) rectangular unit cell shown on the *right*)

3.3.4 2D Bravais Lattices

There are five two-dimensional (2D) Bravais lattices (Fig. 3.8) which are distinct and fill all (2D) space. These are very important for the description of symmetries at surfaces. The 2D Bravais lattices are the square, hexagonal, rectangular and centered-rectangular lattice.

3.3.5 3D Bravais Lattices

In three dimensions, the operations of the point group results in fourteen 3D Bravais lattices (Fig. 3.9), that are categorized into seven crystal classes (trigonal, monoclinic,

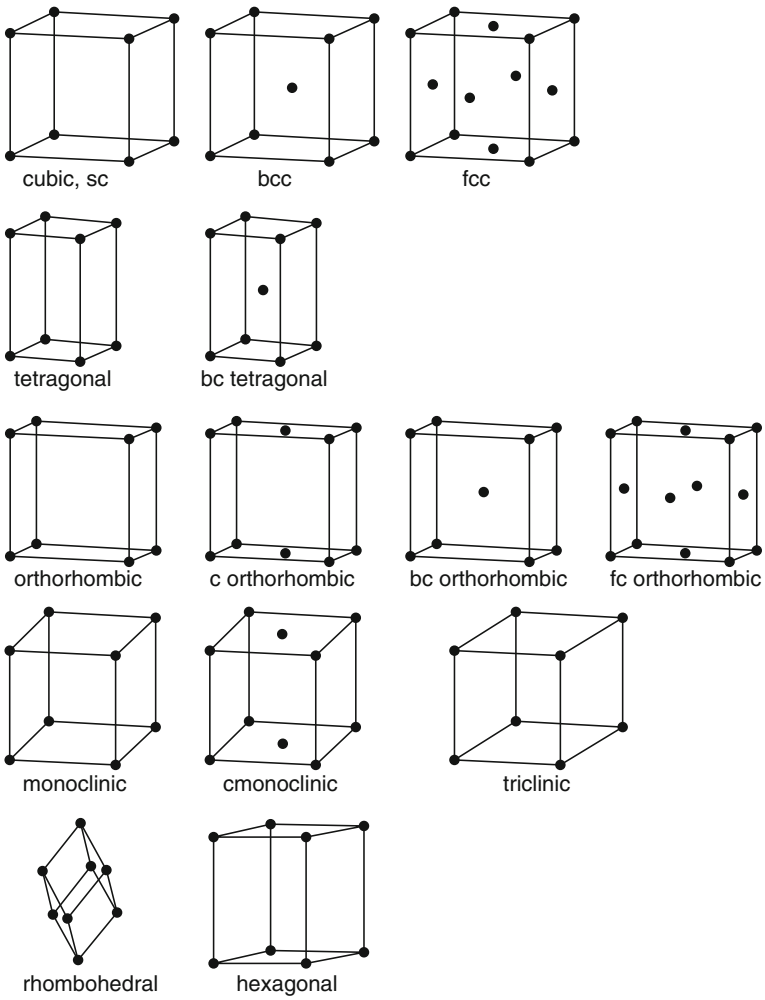

Fig. 3.9 The 14 three-dimensional Bravais lattices: cubic (sc: simple cubic, bcc: body-centered cubic, fcc: face-centered cubic), tetragonal (simple and body-centered), orthorhombic (simple, centered, body-centered and face-centered), monoclinic (simple and centered), triclinic, rhombohedral and hexagonal

rhombic, tetragonal, cubic, rhombohedral and hexagonal). These classes are discerned by the conditions for the lengths and the mutual angles of the vectors that span the lattice (Table 3.1). Some classes have several members. The cubic crystal can have a simple (sc), face-centered (fcc) or body-centered (bcc) lattice.

In the following, some of the most important lattices, in particular those most relevant to semiconductors, will be treated in some more detail.

Table 3.1 Conditions for lengths and angles for the 7 crystal classes

System	#	Lattice symbol	Conditions for the usual unit cell
Triclinic	1		None
Monoclinic	2	s, c	$\alpha = \gamma = 90°$ or $\alpha = \beta = 90°$
Orthorhombic	4	s, c, bc, fc	$\alpha = \beta = \gamma = 90°$
Tetragonal	2	s, bc	$a = b$, $\alpha = \beta = \gamma = 90°$
Cubic	3	s, bc, fc	$a = b = c$, $\alpha = \beta = \gamma = 90°$
Trigonal	1		$a = b$, $\alpha = \beta = 90°$, $\gamma = 120°$
(Rhombohedral)	1		$a = b = c$, $\alpha = \beta = \gamma$
Hexagonal	1		$a = b$, $\alpha = \beta = 90°$, $\gamma = 120°$

Note that only the positive conditions are listed. The rhombohedral system is a special case of the trigonal class. Conditions for the trigonal and hexagonal classes are the same, however, trigonal symmetry includes a single C_3 or S_6 axis, while hexagonal symmetry includes a single C_6 or S_6^5 axis

Cubic fcc and bcc Lattices

The primitive translation vectors for the cubic face-centered (fcc) and the cubic body-centered (bcc) lattice are shown in Figs. 3.10 and 3.11, respectively. Many metals crystallize in these lattices, e.g., copper (fcc) and tungsten (bcc).

In the fcc lattice, one lattice point sits in the center of each of the six faces of the usual cubic unit cell. The vectors spanning the primitive unit cell are

$$\begin{aligned} \mathbf{a}_1 &= \frac{a}{2}\,(1,1,0) \\ \mathbf{a}_2 &= \frac{a}{2}\,(0,1,1) \\ \mathbf{a}_3 &= \frac{a}{2}\,(1,0,1)\,. \end{aligned} \tag{3.2}$$

In the bcc lattice, one extra lattice point sits at the intersection of the three body diagonals at $(\mathbf{a}_1 + \mathbf{a}_2 + \mathbf{a}_3)/2$. The vectors spanning the primitive unit cell are

$$\begin{aligned} \mathbf{a}_1 &= \frac{a}{2}\,(1,1,-1) \\ \mathbf{a}_2 &= \frac{a}{2}\,(-1,1,1) \\ \mathbf{a}_3 &= \frac{a}{2}\,(1,-1,1)\,. \end{aligned} \tag{3.3}$$

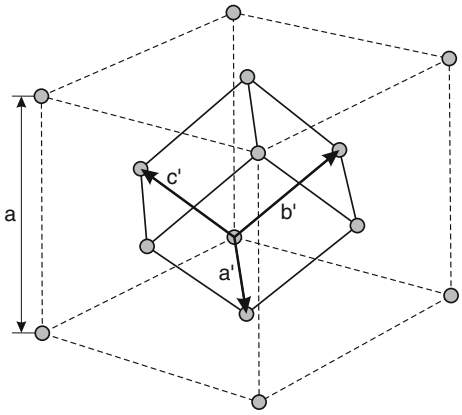

Fig. 3.10 Primitive translations of the fcc lattice. These vectors connect the origin with the face-center points. The primitive unit cell is the rhombohedron spanned by these vectors. The primitive translations $\mathbf{a}'$, $\mathbf{b}'$ and $\mathbf{c}'$ are given in (3.2). The angle between the vectors is 60°

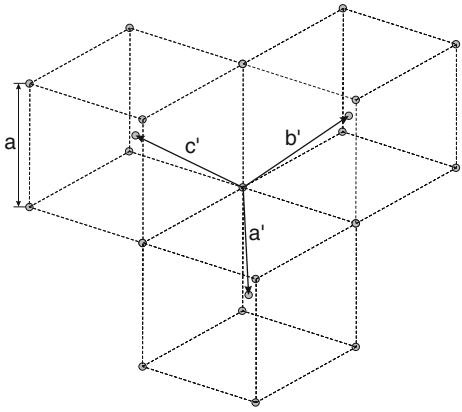

Fig. 3.11 Primitive translations of the bcc lattice. These vectors connect the origin with the lattice points in the cube centers. The primitive unit cell is the rhombohedron spanned by these vectors. The primitive translations $\mathbf{a}'$, $\mathbf{b}'$ and $\mathbf{c}'$ are given in (3.3). The angle between the vectors is ≈70.5°

Hexagonally Close Packed Lattice (hcp)

The 2D hexagonal Bravais lattice fills a plane with spheres (or circles) with maximum filling factor. There are two ways to fill space with spheres and highest filling factor. One is the fcc lattice, the other is the hexagonally close packed (hcp) structure. Both have a filling factor of 74 %.

For the hcp, we start with a hexagonally arranged layer of spheres (A), see Fig. 3.12. Each sphere has six next-neighbor spheres. This could, e.g., be a plane in the fcc perpendicular to the body diagonal. The next plane B is put on top in such a way that each new sphere touches three spheres of the previous layer. The third plane can now be added in two different ways: If the spheres of the third layer are vertically on top of the spheres of layer A, a plane A' identical to A has been created that is shifted from A along the stacking direction (normally called the c-axis) by

$$c_{\mathrm{hcp}} = \sqrt{8/3}\, a \approx 1.633\, a. \tag{3.4}$$

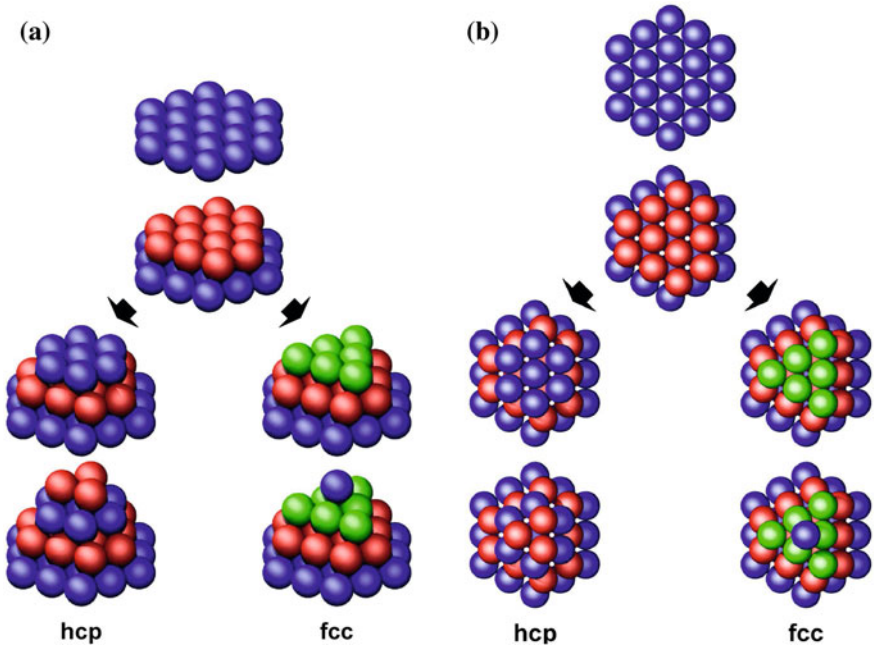

Fig. 3.12 Structure of the (**a**) hcp and (**b**) fcc lattice. For hcp the stacking (along the c-axis) is ABABAB. . ., for fcc (along the body diagonal) it is ABCABCABC. . .

The vectors spanning the primitive unit cell are

$$\begin{aligned} \mathbf{a}_1 &= \frac{a}{2}\left(1, -\sqrt{3}, 0\right) \\ \mathbf{a}_2 &= \frac{a}{2}\left(1, \sqrt{3}, 0\right) \\ \mathbf{a}_3 &= c\ (0, 0, 1)\,. \end{aligned} \tag{3.5}$$

The hcp stacking order is ABABAB. . . for hcp, the coordination number is 12. In the fcc structure, the third layer is put on the thus far unfilled positions and forms a new layer C. Only the forth layer is again identical to A and is shifted by

$$c_{\text{fcc}} = \sqrt{6}\,a \approx 2.45\,a. \tag{3.6}$$

The fcc stacking order is ABCABCABC. . .

In the hexagonal plane of the fcc lattice (which will later be called a {111} plane) the distance between lattice points is $a = a_0/\sqrt{2}$, where a_0 is the cubic lattice constant. Thus $c = \sqrt{3}\,a_0$, just what is expected for the body diagonal.

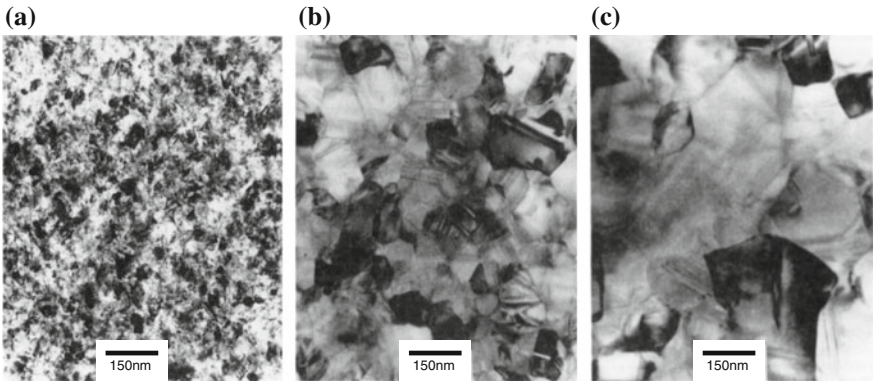

Fig. 3.13 Transmission electron micrographs of polycrystalline silicon (poly-Si). (**a**) As-deposited material from low-pressure chemical vapor deposition (LPCVD) at about 620 °C, grain size is about 30 nm. (**b**) After conventional processing (annealing at 1150 °C), average grain size is about 100 nm. (**c**) After annealing in HCl that provides enhanced point defect injection (and thus increased possibility to form larger grains), average grain size is about 250 nm. Adapted from [172]

For real materials with hexagonal lattice the ratio c/a deviates from the ideal value given in (3.4). Helium comes very close to the ideal value, for Mg it is 1.623, for Zn 1.861. Many hcp metals exhibit a phase transition to fcc at higher temperatures.

3.3.6 Polycrystalline Semiconductors

A polycrystalline material consists of crystal grains that are randomly oriented with respect to each other. Between two grains a (large-angle) grain boundary (see also Sect. 4.4.3) exists. An important parameter is the grain size and its distribution. It can be influenced via processing steps such as annealing. Polycrystalline semiconductors are used in cheap, large-area applications such as solar cells (e.g., polysilicon, $CuInSe_2$) or thin-film transistors (poly-Si) or as n-conducting contact material in MOS diodes (poly-Si) as shown in Fig. 3.13 (see also Fig. 21.28). Polycrystalline material can be fabricated from amorphous material using annealing procedures as discussed in Sect. 24.6.1 for silicon.

3.3.7 Amorphous Semiconductors

An amorphous material lacks the long-range order of the direct lattice. It is disordered on the atomic scale. Historically, amorphous Se (a-Se) has been investigated first; since the 1950s amorphous chalcogenides and a-Ge [173] and since the late 1960s a-Si [174] are researched. The field of amorphous oxides started in the mid 1950s

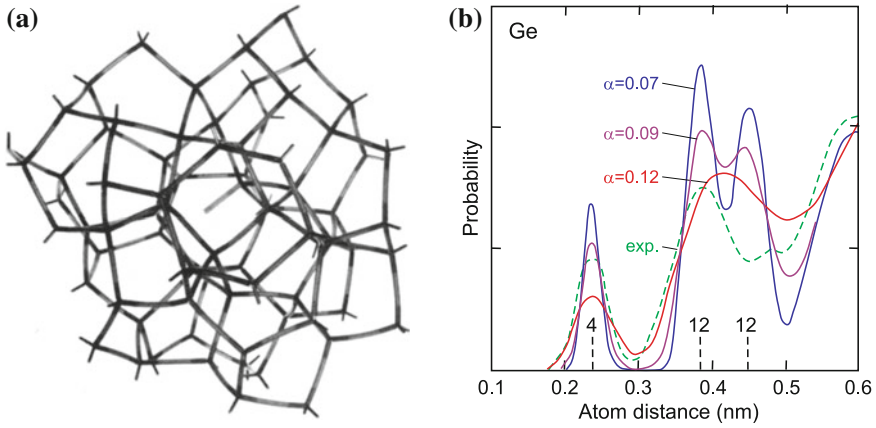

Fig. 3.14 (**a**) A continuous random network model of amorphous silicon containing a dangling bond in the center of the figure. Reprinted with permission from [178]. (**b**) Calculated radial atomic distribution functions of amorphous Ge (*solid lines*) for three different values of the disorder parameter α (3.7) as labeled and experimental result (*dashed line*). The positions of next, second-next and third-next neighbors are indicted by *vertical bars* with numbers of their multiplicity (4, 12, and 12). Adapted from [177]

with vanadates [175] and is currently very active with mixed-metal-based oxides [176] (cmp. Chap. 20).

The local quantum mechanics provides almost rigorous requirements for the bond length to next neighbors. The constraints for the bond angle are less strict. Covalently bonded atoms arrange in an open network with correlations up to the third and fourth neighbors. The short-range order is responsible for the observation of semiconductor properties such as an optical absorption edge and also thermally activated conductivity. In Fig. 3.14a a model of a continuous random network (with a bond-angle distortion of less than about 20 %) of a-Si is depicted. The diameter d_{SR} of the short-range order region is related to the disorder parameter α via [177]

$$d_{\mathrm{SR}} = \frac{a}{2\,\alpha}, \tag{3.7}$$

where a is the next-neighbor interatomic distance. For a diamond structure it is related to the lattice constant by $a = \sqrt{3}\,a_0/4$.

Typically, a significant number of dangling bonds exists. Bonds try to pair but if an odd number of broken bonds exists locally, an unsaturated, dangling bond remains. This configuration can be passivated by a hydrogen atom. Thus, the hydrogenation of amorphous semiconductors is very important, in particular for a-Si. A hydrogen atom can also break an overlong (and therefore weak) bond, saturate one side and eventually leave a dangling bond.

Amorphous material can be (re-)crystallized into crystalline, mostly polycrystalline material upon annealing. This is technologically very important for a-Si (see Sect. 24.6.1).

3.4 Important Crystal Structures

Now the crystal structures that are important for semiconductor physics will be discussed. These are mainly the rocksalt (PbS, CdO, ...), diamond (C, Si, Ge), zincblende (GaAs, InP, ...) and wurtzite (GaN, ZnO, ...) structures.

3.4.1 Rocksalt Structure

The rocksalt (rs, NaCl, space group 225, $Fm\bar{3}m$) structure (Fig. 3.15a) consists of a fcc lattice with the period a and a diatomic base in which the Cl atom is positioned at (0, 0, 0) and the Na atom at (1/2, 1/2, 1/2)a with a distance $\sqrt{3}\,a/2$. Materials that crystallize (under normal conditions) in the rocksalt lattice are, e.g., KCl, KBr, PbS (galena), PbSe, PbTe, AgBr, MgO, CdO, MnO. AlN, GaN and InN undergo, under high pressure, a phase transition from the wurtzite into the rocksalt structure.

3.4.2 CsCl Structure

The CsCl structure (space group 221, $Pm\bar{3}m$) (Fig. 3.15b) consists of a simple cubic lattice. Similar as for the rocksalt structure, the base consists of different atoms

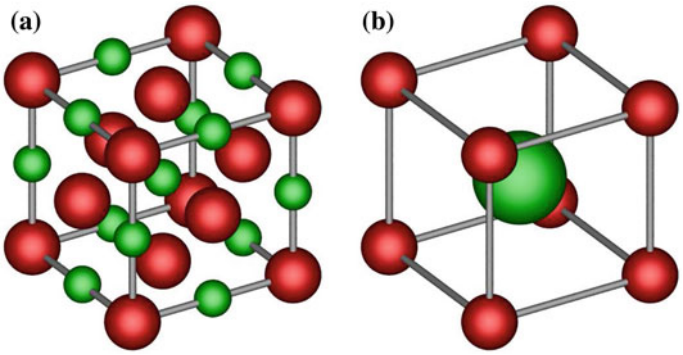

Fig. 3.15 (**a**) Rocksalt (NaCl) structure, (**b**) CsCl structure

at (0, 0, 0) and (1/2, 1/2, 1/2)a. Typical crystals with CsCl-structure are TlBr, TlI, CuZn (β-brass), AlNi.

3.4.3 Diamond Structure

The diamond structure (C, space group 227, Fd$\bar{3}$m) (Fig. 3.16a) has the fcc lattice. The base consists of two identical atoms at (0, 0, 0) and (1/4, 1/4, 1/4)a. Each atom has a tetrahedral configuration. The packing density is only about 0.34. The ABC-type stacking along the [111]-direction is visualized in Fig. 3.17a. The materials that crystallize in the diamond lattice are C, Ge, Si and α-Sn. Silicon as the most important semiconductor is particularly well researched [179].

The diamond structure (point group O_h) has an inversion center, located between the two atoms of the base, i.e. at (1/8, 1/8, 1/8)a. The radii of the wavefunctions for various group-IV elements increases with the order number (Table 3.2), and accordingly the lattice constant increases.

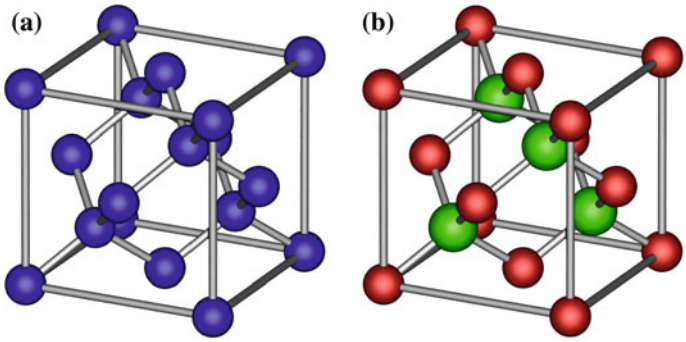

Fig. 3.16 (**a**) Diamond structure and (**b**) zincblende structure (*red spheres*: A atoms, *green spheres*: B atoms). The tetragonal bonds are indicated

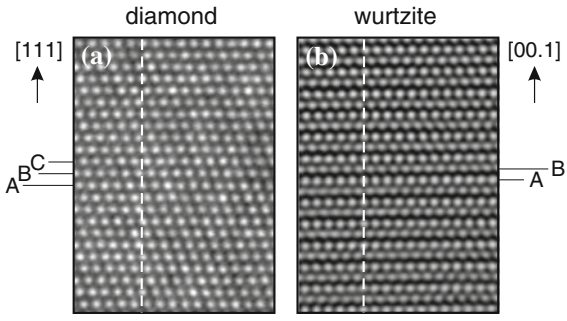

Fig. 3.17 HRTEM images of (**a**) diamond structure (Si, {110} cross section) and (**b**) wurtzite structure (GaN, ⟨10.0⟩ azimuth). The ABC and AB stacking is indicated

Table 3.2 Radii of the wavefunctions in the diamond structure, r_s and r_p are related to s^1p^3, r_d to $s^1p^2d^1$ and lattice constant a_0

	r_s (nm)	r_p (nm)	r_d (nm)	a_0 (nm)
C	0.121	0.121	0.851	0.3567
Si	0.175	0.213	0.489	0.5431
Ge	0.176	0.214	0.625	0.5646

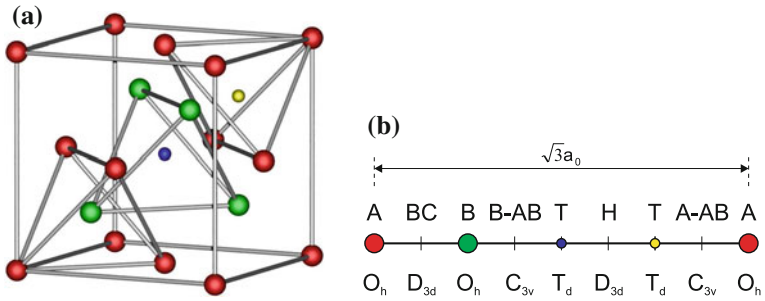

Fig. 3.18 (**a**) Unit cell of the zincblende structure with the indication of tetragonal symmetries. The position of the small *yellow* (*blue*) *sphere* is the tetrahedrally configured unoccupied positions of the A (B) sublattice, denoted with 'T' in part (**b**). (**b**) Line along [111] in the zincblende structure. The positions of the A and B atoms are denoted by *red* and *green circles* as labeled. Other positions are called the bond center ('BC'), antibonding ('AB') relative to A and B atoms ('A–AB', 'B–AB'), hexagonal ('H') and tetrahedral position ('T', *blue* and *yellow circles*)

In Fig. 3.18a the unit cell with tetragonal symmetry of three places along the ⟨111⟩ direction is shown. In Fig. 3.18b the arrangement of atoms along ⟨111⟩ is depicted. The symmetry along this line is at least C_{3v}. At the atoms sites it is O_h. The bond center (BC) and the hexagonal (H) position are a center of inversion and have D_{3d} symmetry. The unoccupied 'T' positions have T_d symmetry. High-pressure phases of silicon are already found in indentation experiments [180].

We note that α-Sn has little current importance. The diamond structure α–Sn phase is stable below 13.2 °C. The addition of Ge inhibits the retransformation to metallic tin up to higher temperatures (e.g., 60 °C for 0.75 weight percent Ge). The properties of gray tin are reviewed in [181].

3.4.4 Zincblende Structure

The zincblende (sphalerite,[4] ZnS, space group 216, F$\bar{4}$3m) structure (Fig. 3.16b) has a fcc lattice with a diatomic base. The metal (A) atom is at (0, 0, 0) and the

[4]Zincblende technically means the material ZnS which occurs in sphalerite (cubic) and wurtzite (hexagonal) phase. However, in the literature the term 'zincblende' for the sphalerite structure is common and used throughout this book.

nonmetal (B) atom is at $(1/4, 1/4, 1/4)a$. Thus the cation and anion sublattices are shifted with respect to each other by a quarter of the body diagonal of the fcc lattice. The atoms are tetrahedrally coordinated, a Zn atom is bonded to four S atoms and vice versa. However, no inversion center is present any longer (point group T_d). In the zincblende structure the stacking order of diatomic planes along the body diagonal is aAbBcCaAbBcC...

Many important compound semiconductors, such as GaAs, InAs, AlAs, InP, GaP and their alloys (cf. Sect. 3.7), but also the II–VI compounds ZnS, ZnSe, ZnTe, HgTe and CdTe and halides, including AgI, CuF, CuCl, CuBr, and CuI, crystallize in the zincblende structure.

Four-fold coordinated materials (zincblende and wurtzite) typically undergo a phase transition into 6-fold coordinated structures upon hydrostatic pressure [182]. For GaAs under pressure see [183].

3.4.5 *Wurtzite Structure*

The wurtzite structure (ZnS, space group 186, $P6_3mc$) is also called the hexagonal ZnS structure (because ZnS has both modifications). It consists (Fig. 3.19) of a hcp lattice with a diatomic base. The c/a ratio typically deviates from the ideal value $\zeta_0 = \sqrt{8/3} \approx 1.633$ (3.4) as listed in Table 3.3. The c-axis is a 6_3 screw axis.

The Zn atom is located at (0, 0, 0), the S atom at $(0, 0, \sqrt{3/8})a$. This corresponds to a shift of $3/8\,c$ along the c-axis. This factor is called the cell-internal parameter u. For real wurtzite crystals u deviates from its ideal value $u_0 = 3/8 = 0.375$, e.g., for group-III nitrides $u > u_0$. The diatomic planes have a stacking order of aAbBaAbB... along the [00.1]-direction as visualized in Fig. 3.17b.

In Fig. 3.20 the different local structural environment of the atoms in the zincblende and wurtzite structure is shown.

Many important semiconductors with large band gap crystallize in the wurtzite structure, such as GaN, AlN, InN, [185] ZnO, [186] SiC, [187], CdS und CdSe.

Table 3.3 c/a ratio of various wurtzite semiconductors

Material	ξ (%)	Material	ξ(%)	Material	ξ (%)	Material	ξ (%)
AlN	−2.02	CdS	−0.61	CuBr	0.43	BeO	−0.61
GaN	−0.49	CdSe	−0.18	CuCl	0.55	ZnO	−1.9
InN	−1.35	CdTe	0.25	CuI	0.74	6H-SiC	0.49
ZnS	0.25	MgS	−0.80	AgI	0.12	BN	0.74
ZnSe	0.06	MgSe	−0.67	ZnTe	0.74	MgTe	−0.67

Listed is $\xi = (c/a - \zeta_0)/\zeta_0$. Data based on [184]

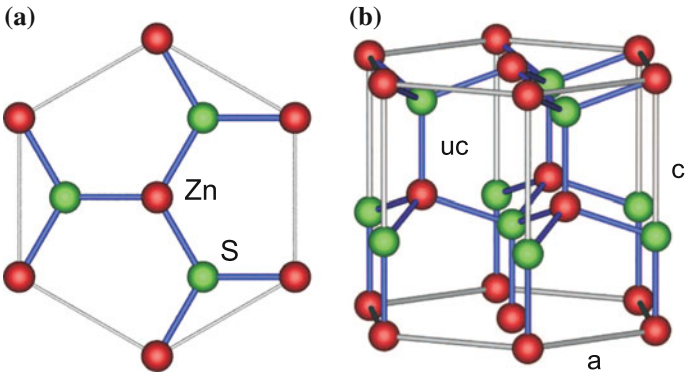

Fig. 3.19 (**a**) *Top view* (along the *c*-axis) and (**b**) *side view* of the wurtzite structure with the tetragonal bonds indicated. The *top* (*bottom*) surface of the depicted structure is termed the Zn-face, (00.1) (O-face, $(00.\bar{1})$)

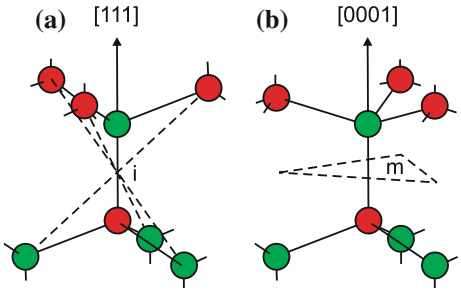

Fig. 3.20 Comparison of the tetragonal bonds in the (**a**) zincblende and (**b**) wurtzite structure (*i*: inversion center, *m*: symmetry plane)

3.4.6 Chalcopyrite Structure

The chalcopyrite [188] (ABC_2, named after 'fool's gold' $CuFeS_2$, space group 122, $I\bar{4}2d$) structure is relevant for I–III–VI_2 (with chalcogenide anions) and II–IV–V_2 (with pnictide anions) semiconductors such as, e.g., $(Cu,Ag)(Al,Ga,In)(S,Se,Te)_2$ and $(Mg,Zn,Cd)(Si,Ge,Sn)(As,P,Sb)_2$. A nonmetallic anion atom ('C') is tetrahedrally bonded to two different types of cation atoms ('A' and 'B') as shown in Fig. 3.21. The local surrounding of each anion is identical, two of both the A and B atoms. The structure is tetragonal. The aspect ratio $\eta = c/(2a)$ deviates from its ideal value 1; typically $\eta < 1$ [189, 190].

If the C atom is in the tetrahedral center of the two A and two B atoms, the bond lengths R_{AC} and R_{BC} of the A–C and B–C bonds, respectively, are equal. Since the ideal A–C and B–C bond lengths d_{AC} and d_{BC} are typically unequal, this structure is strained. The common atom C is therefore displaced along [100] and [010] such

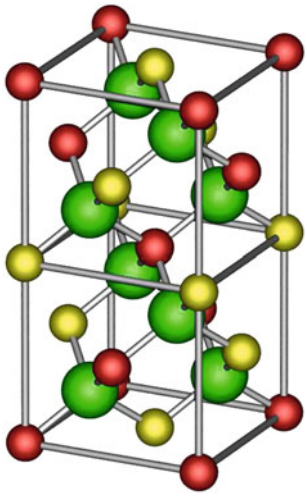

Fig. 3.21 Chalcopyrite structure, *red* and *yellow spheres* denote the metal species. The bigger *green spheres* represent the nonmetal anion

that it is closer (if $d_{AC} < d_{BC}$) to the pair of A atoms and further away from the B atoms. The displacement parameter is

$$u = \frac{1}{4} + \frac{R_{AC}^2 - R_{BC}^2}{a^2} \tag{3.8}$$

and it deviates from the ideal value $u_0 = 1/4$ for the zincblende structure as listed in Table 3.4 for a number of chalcopyrite compounds. In the chalcopyrite structure

$$R_{AC} = a\sqrt{u^2 + \frac{1+\eta^2}{16}} \tag{3.9a}$$

$$R_{BC} = a\sqrt{\left(u - \frac{1}{2}\right)^2 + \frac{1+\eta^2}{16}}. \tag{3.9b}$$

The minimization of the microscopic strain yields (in first order) [191]

$$u \cong \frac{1}{4} + \frac{3}{8}\frac{d_{AC}^2 - d_{BC}^2}{d_{AC}^2 + d_{BC}^2}. \tag{3.10}$$

Compounds with $u > u_c$, $u_c = 0.265$ being a critical displacement parameter, (or $u < 1/2 - u_c = 0.235$) are stable with regard to cation disorder [190]. In Fig. 3.22 the correlation of the calculated value for u according to (3.10) and the experimental values is shown.

Table 3.4 Lattice nonideality parameters η and u (from (3.10)) of various chalcopyrite compounds and their experimentally observed disorder stability (+/− indicates compound with/without order–disorder (D–O) transition, respectively)

	η	u	D–O		η	u	D–O
$CuGaSe_2$	0.983	0.264	+	$ZnSiAs_2$	0.97	0.271	−
$CuInSe_2$	1.004	0.237	+	$ZnGeAs_2$	0.983	0.264	+
$AgGaSe_2$	0.897	0.287	−	$CdSiAs_2$	0.92	0.294	−
$AgInSe_2$	0.96	0.261	+	$CdGeAs_2$	0.943	0.287	
$CuGaS_2$	0.98	0.264		$ZnSiP_2$	0.967	0.272	−
$CuInS_2$	1.008	0.236	+	$ZnGeP_2$	0.98	0.264	+
$AgGaS_2$	0.895	0.288	−	$CdSiP_2$	0.92	0.296	−
$AgInS_2$	0.955	0.262		$CdGeP_2$	0.939	0.288	−

Data from [190]

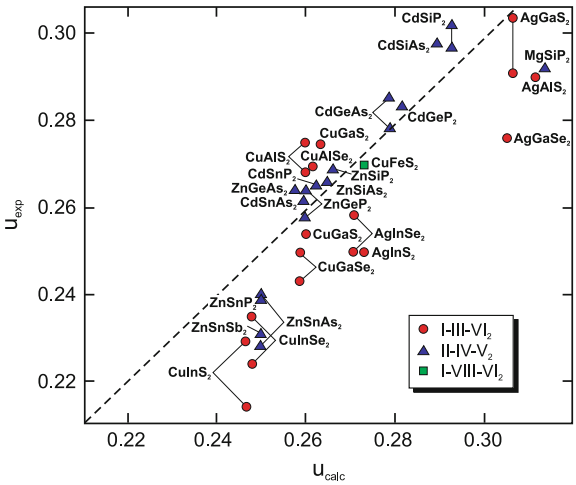

Fig. 3.22 Experimental values u_{exp} of the displacement parameter for various chalcopyrites versus the calculated value u_{calc} according to (3.10). The *dashed line* indicates $u_{exp} = u_{calc}$. Adapted from [191]

3.4.7 Spinel Structure

A large variety of ternary compounds of type $A^{II}B^{III}{}_2C^{VI}{}_4$ crystallize in the cubic spinel structure (spinel, $MgAl_2O_4$, space group 227, Fd3m). Typical elements are A: Mg, Cr, Mn, Fe, Co, Ni, Cu, Zn, Cd, Sn, B: Al, Ga, In, Ti, V, Cr, Mn, Fe, Co, Rh, Ni, and C: O, S, Se, Te.

As an example $ZnGa_2O_4$ (zinc gallate) has received attention as interfacial layer in ZnO/GaAs epitaxy [192], luminescent material [193], and as ferromagnetic semiconductor [194]. Also the (unwanted) appearance of zinc gallate inclusions is in

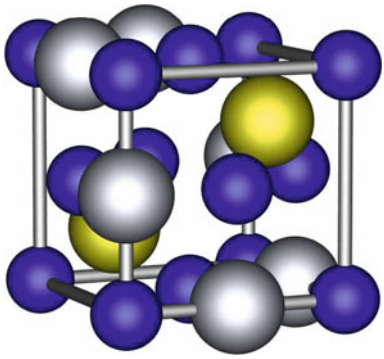

Fig. 3.23 Spinel AB_2C_4 crystal structure, the cations are depicted as *yellow* (A atoms) and *silver* (B atoms) *spheres*, the anions (C atoms) as *blue spheres*

competition with the formation of highly doped wurtzite ZnO:Ga; in the (normal) spinel cubic structure of $ZnGa_2O_4$ the Zn^{2+} ions still occupy tetrahedral sites, but the Ga^{3+} ions occupy octahedral sites instead of tetrahedral sites in doped wurtzite ZnO:Ga. (Sc,Al)MgO_4 (SCAM) is available as substrate material. Also $A^{VI}B^{II}{}_2C^{VI}{}_4$ compounds exist, e.g., GeB_2O_4 (with B = Mg, Fe, Co, Ni)

The anion atoms (C^{2-}) sit on a fcc lattice. The A atoms fill 1/8 of all tetraeder spaces and the B atoms fill half of all octaeder places (Fig. 3.23). Often the cations are charged A^{2+} and B^{3+}, e.g., in $ZnAl_2O_4$, $MgCr_2O_4$ or $ZnCo_2O_4$. Also A^{6+} and B^{1-} exists, e.g., in WNa_2O_4.

The cubic lattice constant is denoted as a. In real spinels, the anions deviate from the ideal fcc array which is accounted for by the parameter u, measuring the displacement of anions along the [111]-direction [195]; if the A-site cation is at (0,0,0), an anion is at (u, u, u). The cation-anion distances are given by [196]

$$R_{AC} = a\sqrt{3\,(u - 1/8)}, \tag{3.11a}$$

$$R_{BC} = a\sqrt{3\,u^2 - 2\,u - 3/8}. \tag{3.11b}$$

The ideal value is $u = 1/4$; examples are $u = 0.2624$ for $MgAl_2O_4$, $u = 0.2617$ for $ZnGa_2O_4$ and $u = 0.2409$ for $SiFe_2O_4$ [196].

In the inverted spinel structure, for $A^{II}B^{III}{}_2C^{VI}{}_4$ compounds, the cations are distributed like $B(AB)C_4$, i.e. the B cations occupy tetraeder and octaeder places, e.g., in $Mg^{2+}(Mg^{2+}Ti^{4+})O_4^{2-}$ or $Fe^{3+}(Ni^{2+}Fe^{3+})O_4^{2-}$. Examples are magnetite (Fe_3O_4), a material with high spin polarization, or $MgFe_2O_4$. Also $A^{VI}B^{II}{}_2C^{VI}{}_4$ compounds exist in this structure, e.g., SnB_2O_4 (with B = Mg, Mn, Co, Zn), TiB_2O_4 (with B = Mg, Mn, Fe, Co, Zn), and VB_2O_4 (with B = Mg, Co, Zn).

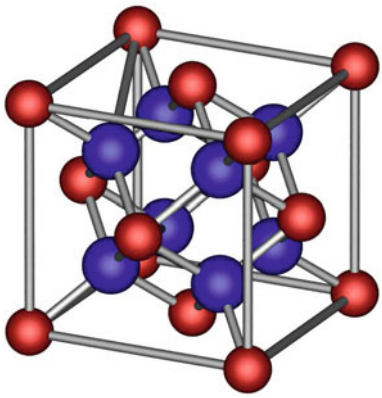

Fig. 3.24 Fluorite crystal structure, the cations are depicted as *red spheres*, the anions as *blue spheres*

3.4.8 Fluorite Structure

Named after the minerale fluorite (CaF_2, space group 225, Fm3m), this structure for binary ionic compounds occurs when the cation valence is twice the anion valence, e.g., for (cubic) ZrO_2 (zirconia) or HfO_2. The lattice is fcc with a triatomic base. At (0,0,0) is the cation (e.g., Zr^{4+}), the anions (e.g., O^{2-}) are at (1/4, 1/4, 1/4) a (as in the zincblende structure) and (3/4, 3/4, 3/4) a (Fig. 3.24). The anion atom positions are on a simple cubic lattice with lattice constant $a/2$. Zirconia can crystallize in various phases [197], the most prominent being the monoclinic, tetragonal and cubic phases. The cubic phase can be extrinsically stabilized using yttrium [198, 199] (YSZ, yttria-stabilized zirconia). Hafnium oxide has the remarkable property that the HfO_2/Si interface is stable and allows the fabrication of transistor gate oxides with high dielectric constant (see Sect. 24.5.5).

3.4.9 Delafossite Structure

The I–III–O_2 materials crystallize in the trigonal delafossite ($CuFeO_2$, space group 166, $R\bar{3}m$) structure (Fig. 3.25). This structure is also called caswellsilverite ($NaCrS_2$). In Table 3.5 the lattice parameters of some delafossite compounds are given. The (Cu, Ag) (Al, Ga, In)O_2 materials are transparent conductive oxides (TCO). We note that Pt and Pd as group-I component create metal-like compounds because of the d^9 configuration as opposed to the d^{10} configuration of Cu and Ag.

3.4.10 Perovskite Structure

The perovskite structure for ABO: 3 materials (calcium titanate, $CaTiO_3$, space group 62, Pnma) (Fig. 3.26) is relevant for ferroelectric semiconductors (cf. Sect. 15.3). It is cubic with the Ca (or Ba, Sr) ions (charge state 2+) on the corners of the

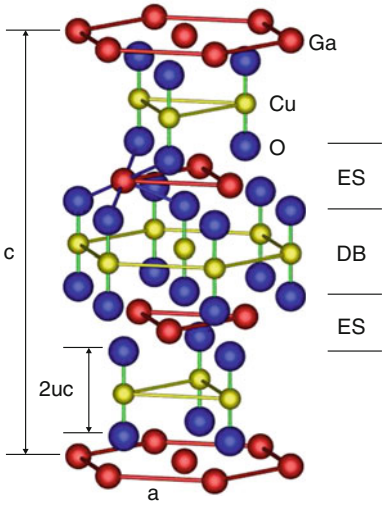

Fig. 3.25 Hexagonal unit cell of delafossite $CuGaO_2$. Oxygen atoms are bonded to the Cu in a dumbbell ('DB') configuration. In the edge-sharing ('ES') layer the Ga atoms are octahedrally configured as GaO_6

Table 3.5 Lattice parameters a, c, and u of some delafossite compounds

	a (nm)	c (nm)	u (nm)
$CuAlO_2$	0.2858	1.6958	0.1099
$CuGaO_2$	0.2980	1.7100	0.1073*
$CuInO_2$	0.3292	1.7388	0.1056*

Theoretical values are shown with asterisk. Data from [200]

cube, the O ions (2−) on the face centers and the Ti (4+) in the body center. The lattice is simple cubic, the base is Ca at (0, 0, 0), O at (1/2, 1/2, 0), (1/2, 0, 1/2) and (0, 1/2, 1/2) and Ti at (1/2, 1/2, 1/2). The ferroelectric polarization is typically evoked by a shift of the negatively and positively charged ions relative to each other. $LaAlO_3$ (lanthanium aluminate) is available as substrate material (space group 226, $Fm\bar{3}c$ [201]). Perovskites are also important for high temperature superconductivity.

3.4.11 NiAs Structure

The NiAs structure (space group 194, $P6_3/mmc$) (Fig. 3.27) is relevant for magnetic semiconductors, such as MnAs, and also occurs in the formation of Ni/GaAs Schottky contacts [202]. The structure is hexagonal. The arsenic atoms form a hcp structure and are trigonal prismatically configured with six nearest metal atoms. The metal atoms form hcp planes and fill all octahedral holes of the As lattice. For a cubic close

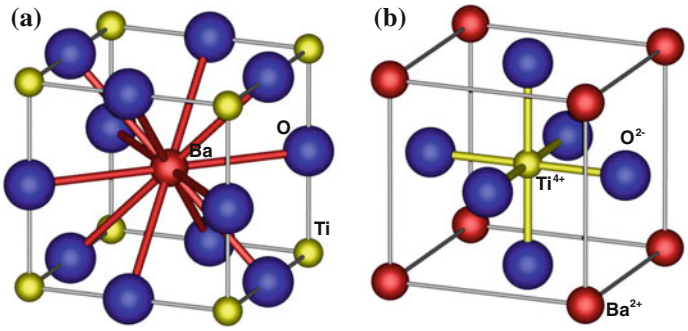

Fig. 3.26 Perovskite structure ($BaTiO_3$), (**a**) A cell with 12-fold (cuboctahedrally) configured Ba, (**b**) B cell with octahedrally configured Ti

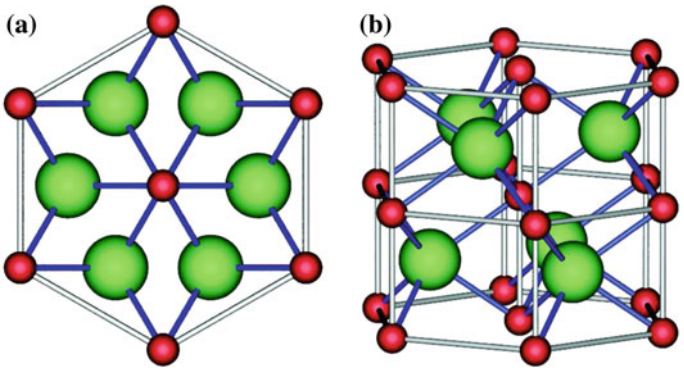

Fig. 3.27 NiAs structure, metal atoms: *dark grey*, chalcogenide atoms: *light grey*

packed, i.e. fcc, structure this would correspond to the rocksalt crystal. The stacking is ABACABAC… (A: Ni, B,C: As).

3.4.12 Further Structures

There are many other crystal structures that have relevance for semiconductor materials. Among them are the

- corundum structure (Al_2O_3, space group 167, $R\bar{3}c$) occurring, e.g., for sapphire substrates used in epitaxy or for gallium oxide α-Ga_2O_3 (Ga_2O_3 is a multiphase material [203])
- bixbyite structure (In_2O_3, δ-Ga_2O_3, space group 206, $Ia\bar{3}$) (see Fig. 20.3)
- β-Ga_2O_3 monoclinic structure (space group 12, C2/m)
- quartz (SiO_2) structures, α-quartz (space group 154, $P3_221$) and β-quartz (space group 180, $P6_222$)

Space does not permit to discuss these and other structures in more detail here. The reader should refer to textbooks on crystallography, e.g., [204–206], and space groups [171, 207]. A good source for information and images of crystal structures on the web is [208].

3.5 Polytypism

In polytype materials the stacking order is not only hcp or fcc but takes different sequences, such as, e.g., ACBCABAC as the smallest unit cell along the stacking direction. A typical example is SiC, for which in addition to hcp and fcc 45 other stacking sequences are known. The largest primitive unit cell of SiC [187] contains 594 layers. Some of the smaller polytypes are sketched in Fig. 3.28. In Fig. 3.29 cubic

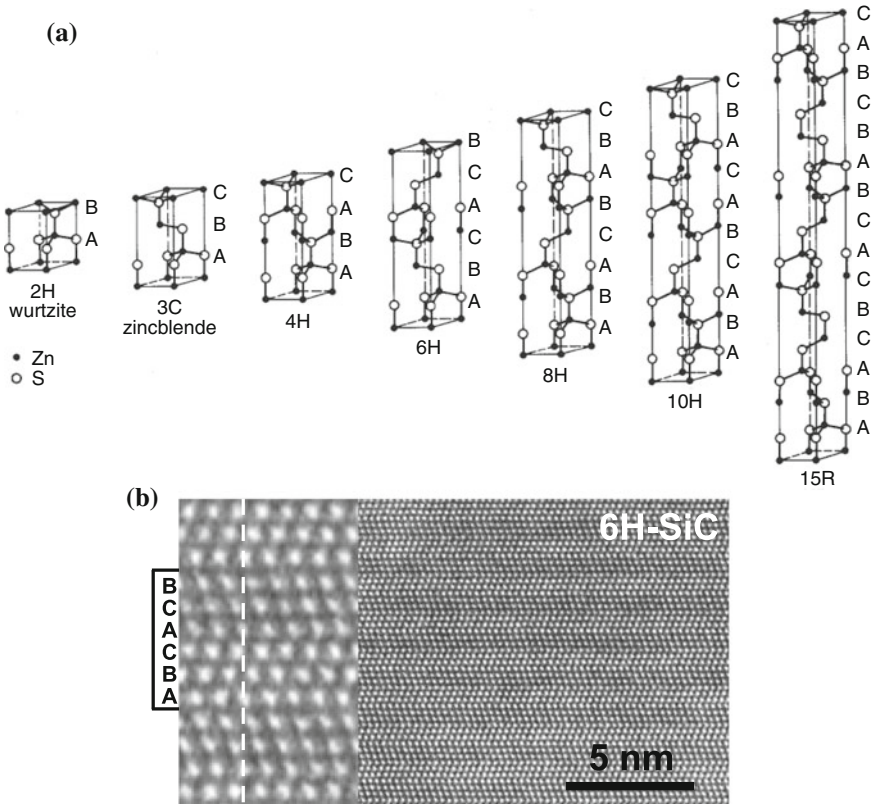

Fig. 3.28 (**a**) Polytypes of the zincblende and wurtzite lattice (found in SiC), the letters A, B and C denote the three possible positions of the diatomic layers (see Fig. 3.12). (**b**) High resolution TEM image of 6H-SiC. For the enlarged view on the *left*, the unit cell and the stacking sequence are indicated. Adapted from [209]

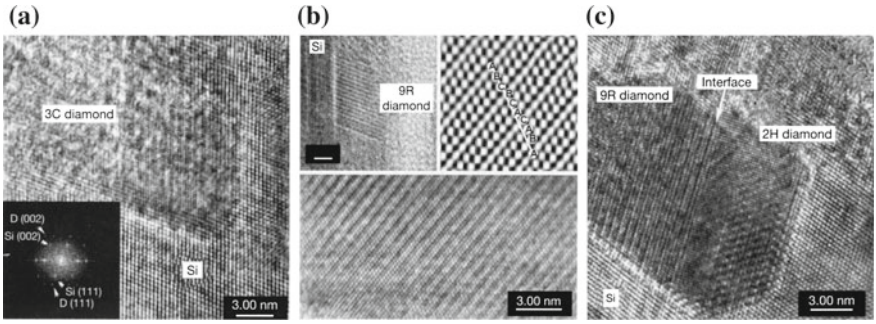

Fig. 3.29 Polytypes of diamond found in crystallites (metastable phases in silicon). (**a**) cubic type (3C) with stacking ABC, *inset* shows a diffractogram and the alignment of the C and Si lattice, (**b**) rhombohedral 9R crystallite with ABCBCACABA stacking, (**c**) 9R phase with interface to a hexagonal 2H (AB stacking) phase. Reprinted with permission from Nature [210], © 2001 Macmillan Magazines Limited

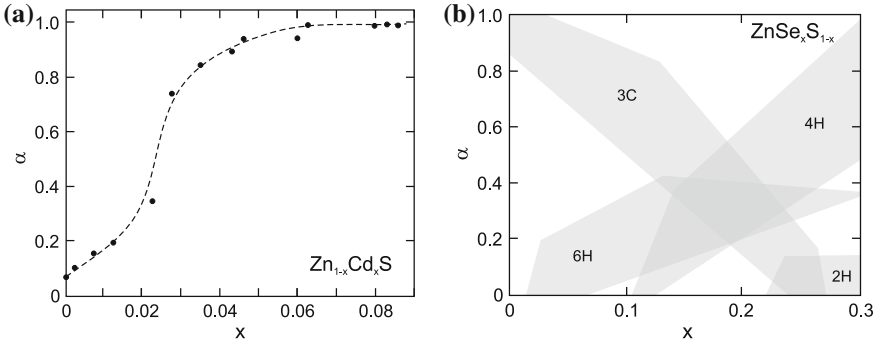

Fig. 3.30 (**a**) Hexagonality index α (3.12) of $Zn_{1-x}Cd_xS$ for various ternary compositions. *Dashed line* is a guide to the eye. (**b**) Regions of different polytypes in $ZnSe_xS_{1-x}$. Adapted from [211]

diamond crystallites and metastable hexagonal and orthorhombic phases (in silicon) are shown.

For the ternary alloy (cf. Sect. 3.7) $Zn_{1-x}Cd_xS$ the numbers n_h of diatomic layers with hexagonal stacking (AB) and n_c of layers with cubic stacking (ABC) have been investigated. CdS has wurtzite structure and ZnS mostly zincblende structure. The hexagonality index α as defined in (3.12) is shown in Fig. 3.30 for $Zn_{1-x}Cd_xS$

$$\alpha = \frac{n_h}{n_h + n_c}. \tag{3.12}$$

3.6 Reciprocal Lattice

The reciprocal lattice is of utmost importance for the description and investigation of periodic structures, in particular for X-ray diffraction [212], surface electron diffraction, phonons and the band structure. It is the quasi-Fourier transformation of the crystal lattice. The crystal lattice is also called the *direct* lattice, in order to distinguish it from the reciprocal lattice.

3.6.1 Reciprocal Lattice Vectors

When $\mathcal{R}$ denotes the set of vectors of the direct lattice, the set $\mathcal{G}$ of the reciprocal lattice vectors is given by the condition[5]

$$\exp(\mathrm{i}\,\mathbf{G}\cdot\mathbf{R}) = 1 \tag{3.13}$$

for all $\mathbf{R} \in \mathcal{R}$ and $\mathbf{G} \in \mathcal{G}$. Therefore, for all vectors $\mathbf{r}$ and a reciprocal lattice vector $\mathbf{G}$

$$\exp(\mathrm{i}\,\mathbf{G}\cdot(\mathbf{r}+\mathbf{R})) = \exp(\mathrm{i}\,\mathbf{G}\cdot\mathbf{r})\,. \tag{3.14}$$

Each Bravais lattice has a certain reciprocal lattice. The reciprocal lattice is also a Bravais lattice, since when $\mathbf{G}_1$ and $\mathbf{G}_2$ are two reciprocal lattice vectors, then this is obviously true also for $\mathbf{G}_1 + \mathbf{G}_2$. For the primitive translation vectors $\mathbf{a}_1$, $\mathbf{a}_2$ and $\mathbf{a}_3$ of the direct lattice, the vectors $\mathbf{b}_1$, $\mathbf{b}_2$ and $\mathbf{b}_3$ that span the reciprocal lattice can be given directly as

$$\mathbf{b}_1 = \frac{2\pi}{V_a}(\mathbf{a}_2 \times \mathbf{a}_3) \tag{3.15a}$$

$$\mathbf{b}_2 = \frac{2\pi}{V_a}(\mathbf{a}_3 \times \mathbf{a}_1) \tag{3.15b}$$

$$\mathbf{b}_3 = \frac{2\pi}{V_a}(\mathbf{a}_1 \times \mathbf{a}_2), \tag{3.15c}$$

where $V_a = \mathbf{a}_1 \cdot (\mathbf{a}_2 \times \mathbf{a}_3)$ is the volume of the unit cell spanned by the vectors $\mathbf{a}_i$. The volume of the unit cell in the reciprocal space is $V_a^* = (2\pi)^3 / V_a$.

The vectors $\mathbf{b}_i$ fulfill the conditions

$$\mathbf{a}_i \cdot \mathbf{b}_j = 2\pi\,\delta_{ij}. \tag{3.16}$$

Thus, it is clear that (3.13) is fulfilled. For an arbitrary reciprocal lattice vector $\mathbf{G} = k_1\mathbf{b}_1 + k_2\mathbf{b}_2 + k_3\mathbf{b}_3$ and a vector $\mathbf{R} = n_1\mathbf{a}_1 + n_2\mathbf{a}_2 + n_3\mathbf{a}_3$ in direct space

[5] The dot product $\mathbf{a} \cdot \mathbf{b}$ of two vectors shall also be denoted as $\mathbf{ab}$.

we find

$$\mathbf{G} \cdot \mathbf{R} = 2\pi \ (n_1 k_1 + n_2 k_2 + n_3 k_3) \,. \tag{3.17}$$

The number in brackets is an integer. Additionally, we note that the reciprocal lattice of the reciprocal lattice is again the direct lattice. The reciprocal lattice of the fcc is bcc and vice versa. The reciprocal lattice of hcp is hcp (rotated by 30° with respect to the direct lattice).

For later, we note two important theorems. A (sufficiently well behaved) function $f(\mathbf{r})$ that is periodic with the lattice, i.e. $f(\mathbf{r}) = f(\mathbf{r} + \mathbf{R})$ can be expanded into a Fourier series with the reciprocal lattice vectors according to

$$f(\mathbf{r}) = \sum a_{\mathbf{G}} \ \exp(\mathrm{i}\,\mathbf{G} \cdot \mathbf{r}), \tag{3.18}$$

where $a_{\mathbf{G}}$ denotes the Fourier component of the reciprocal lattice vector $\mathbf{G}$, $a_{\mathbf{G}} = \int_V f(\mathbf{r}) \exp(-\mathrm{i}\,\mathbf{G} \cdot \mathbf{r})\, \mathrm{d}^3\mathbf{r}$. If $f(\mathbf{r})$ is lattice periodic, the integral given in (3.19) is zero unless $\mathbf{G}$ is a reciprocal lattice vector.

$$\int_V f(\mathbf{r}) \ \exp(-\mathrm{i}\,\mathbf{G} \cdot \mathbf{r}) \ \mathrm{d}^3\mathbf{r} = \begin{cases} a_{\mathbf{G}} \\ 0, \mathbf{G} \notin \mathcal{G} \end{cases} . \tag{3.19}$$

3.6.2 Miller Indices

A lattice plane is the set of all lattice points in a plane spanned by two independent lattice vectors $\mathbf{R_1}$ and $\mathbf{R_2}$. The lattice points on that plane form a two-dimensional Bravais lattice. The entire lattice can be generated by shifting the lattice plane along its normal $\mathbf{n} = (\mathbf{R_1} \times \mathbf{R_2})/|\mathbf{R_1} \times \mathbf{R_2}|$. The plane belongs to the reciprocal lattice vector $\mathbf{G_n} = 2\pi\mathbf{n}/d$, d being the distance between planes.

This correspondence between reciprocal lattice vectors and sets of planes allows the orientation of planes to be described in a simple manner. The shortest reciprocal lattice vector perpendicular to the plane is used. The coordinates with respect to the primitive translation vectors of the reciprocal space $\mathbf{b}_i$ form a triplet of integer numbers and are called Miller indices [213].

The plane described by $\mathbf{G_n} \cdot \mathbf{r} = A$ fulfills the condition for a suitable value of A. The plane intersects the axes $\mathbf{a}_i$ at the points $x_1\,\mathbf{a}_1$, $x_2\,\mathbf{a}_2$ and $x_3\,\mathbf{a}_3$. Thus we find $\mathbf{G_n}\, x_i\, \mathbf{a}_i = A$ for all i. From (3.17) follows $\mathbf{G_n} \cdot \mathbf{a}_1 = 2\pi\, h$, $\mathbf{G_n} \cdot \mathbf{a}_2 = 2\pi\, k$ and $\mathbf{G_n} \cdot \mathbf{a}_3 = 2\pi\, l$, where h, k and l are integers. The triplet of integer numbers (hkl), the reciprocal values of the axis intersections in the direct lattice, are the Miller indices. An example is shown in Fig. 3.31.

Planes are denoted as (hkl) with parentheses. The (outward) normal direction is denoted with $[hkl]$ (square brackets). A set of equivalent planes is denoted with curly brackets as $\{hkl\}$. For example, in the simple cubic lattice (100), (010), (001),

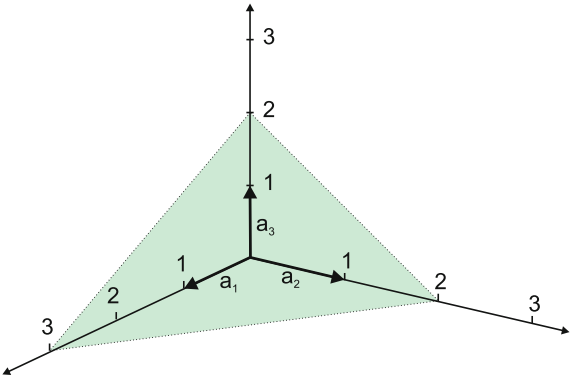

Fig. 3.31 The plane intersects the axes at 3, 2, and 2. The inverse of these numbers is 1/3, 1/2, and 1/2. The smallest integer numbers of this ratio form the Miller indices (233)

(-100), $(0-10)$ are $(00-1)$ equivalent and are denoted by $\{100\}$. (-100) can also be written as $(\bar{1}00)$. A set of equivalent directions is denoted with $\langle hkl \rangle$.

In a cubic lattice the faces of the cubic unit cell are $\{001\}$ and the planes perpendicular to the area (body) diagonals are $\{110\}$ ($\{111\}$) (Fig. 3.32a). In the zincblende lattice the $\{111\}$ planes consist of diatomic planes with Zn and S atoms. It depends on the direction whether the metal or the nonmetal is on top. These two cases are denoted by A and B. We follow the convention that the (111) plane is (111)A and the metal is on top (as in Fig. 3.16b). For each change of sign the type changes from A to B and vice versa, e.g., (111)A, $(1\bar{1}\,1)$B and $(\bar{1}\,\bar{1}\,\bar{1})$B. In Fig. 3.32b the in-plane directions for the (001), (110) and (111) planes are visualized.

In the wurtzite lattice the Miller indices are denoted as $[hklm]$ (Fig. 3.33). Within the (0001) plane three indices hkl are used that are related to the three vectors $\mathbf{a}_1$, $\mathbf{a}_2$ and $\mathbf{a}_3$ (see Fig. 3.33a) rotated with respect to each other by 120°. Of course, the four indices are not independent and $l = -(h + k)$. The third (redundant) index can be denoted as a dot. The c-axis [0001] is then denoted as [00.1]. Wurtzite (and trigonal, e.g., sapphire) substrates are available typically with a ($\langle 11.0 \rangle$), r ($\langle 01.2 \rangle$), m ($\langle 01.0 \rangle$) and c ([00.1]) surface orientations (Fig. 3.33b).

The distance of lattice planes $d = 2\pi/|\mathbf{G}|$ can be expressed via the Miller indices for cubic (3.20a), tetragonal (3.20b) and hexagonal (3.20c) crystals as

$$d^{\mathrm{c}}_{hkl} = \frac{a}{\sqrt{h^2 + k^2 + l^2}} \tag{3.20a}$$

$$d^{\mathrm{t}}_{hkl} = \frac{a}{\sqrt{h^2 + k^2 + l^2\,(a/c)^2}} \tag{3.20b}$$

$$d^{\mathrm{h}}_{hkl} = \frac{a}{\sqrt{4\,(h^2 + hk + k^2)/3 + l^2\,(a/c)^2}} \tag{3.20c}$$

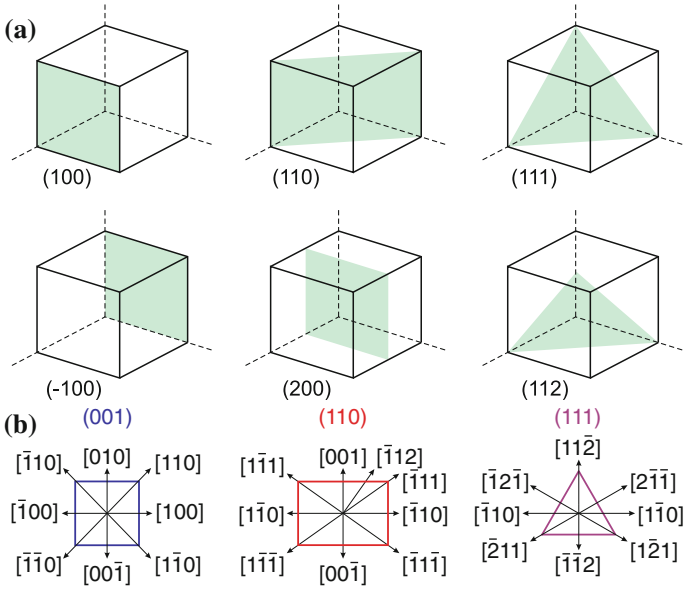

Fig. 3.32 (**a**) Miller indices of important planes for the simple cubic (and fcc, bcc) lattice. (**b**) Directions within three low index planes of cubic crystals

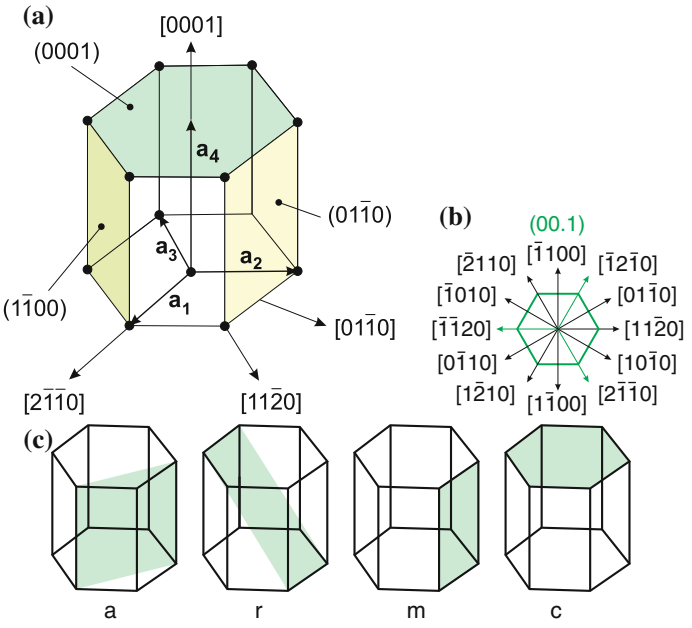

Fig. 3.33 (**a**, **b**) Miller indices for the wurtzite (or hcp) structure. (**c**) Orientation of the a-, r-, m-, and c-plane in the wurtzite structure

Table 3.6 High symmetry points and directions from Γ-point in the Brillouin zone of the fcc lattice

Point	**k**	Direction	$(0 \leq \lambda \leq 1)$
Γ	(0,0,0)		
X	$\frac{2\pi}{a}$ (0, 1, 0)	Δ	$\frac{2\pi}{a}$ (0, λ, 0)
K	$\frac{3\pi}{2a}$ (1, 1, 0)	Σ	$\frac{3\pi}{2a}$ (λ, λ, 0)
L	$\frac{\pi}{a}$ (1, 1, 1)	Λ	$\frac{\pi}{a}$ (λ, λ, λ)
W	$\frac{2\pi}{a}$ (1, 1/2, 0)		
U	$\frac{2\pi}{a}$ (1, 1/4, 1/4)		

Table 3.7 High symmetry points and directions from Γ-point in the Brillouin zone of the hcp lattice

Point	**k**	Direction	$(0 \leq \lambda \leq 1)$
Γ	(0,0,0)		
A	2π (0, 0, $\frac{1}{2c}$)	Δ	$\frac{\pi}{c}$ (0, 0, λ)
L	2π (0, $\frac{1}{\sqrt{3}a}$, $\frac{1}{2c}$)		
M	2π (0, $\frac{1}{\sqrt{3}a}$, 0)	Σ	$\frac{2\pi}{\sqrt{3}a}$ (0, λ, 0)
H	2π ($-\frac{1}{3a}$, $\frac{1}{\sqrt{3}a}$, $\frac{1}{2c}$)		
K	2π ($-\frac{1}{3a}$, $\frac{1}{\sqrt{3}a}$, 0)	T	2π ($-\frac{\lambda}{3a}$, $\frac{\lambda}{\sqrt{3}a}$, 0)

Useful formulas for the angle θ between a (hk.l)-plane and the [00.1]-direction in the cubic, tetragonal and wurtzite structures are:

$$\cos\theta^{\mathrm{c}} = \frac{l}{\sqrt{h^2 + k^2 + l^2}} \tag{3.21a}$$

$$\cos\theta^{\mathrm{t}} = \frac{l}{\sqrt{l^2 + \frac{c^2}{a^2}(h^2 + k^2)}} \tag{3.21b}$$

$$\cos\theta^{\mathrm{h}} = \frac{l}{\sqrt{l^2 + \frac{4}{3}\frac{c^2}{a^2}(h^2 + hk + k^2)}}. \tag{3.21c}$$

3.6.3 Brillouin Zone

The Wigner–Seitz cell in reciprocal space is called the (first) Brillouin zone. In Fig. 3.34, the Brillouin zones for the most important lattices are shown. Certain points in the Brillouin zone are labeled with dedicated letters. The Γ point always denotes $\mathbf{k} = 0$ (zone center). Certain paths in the Brillouin zone are labeled with dedicated Greek symbols.

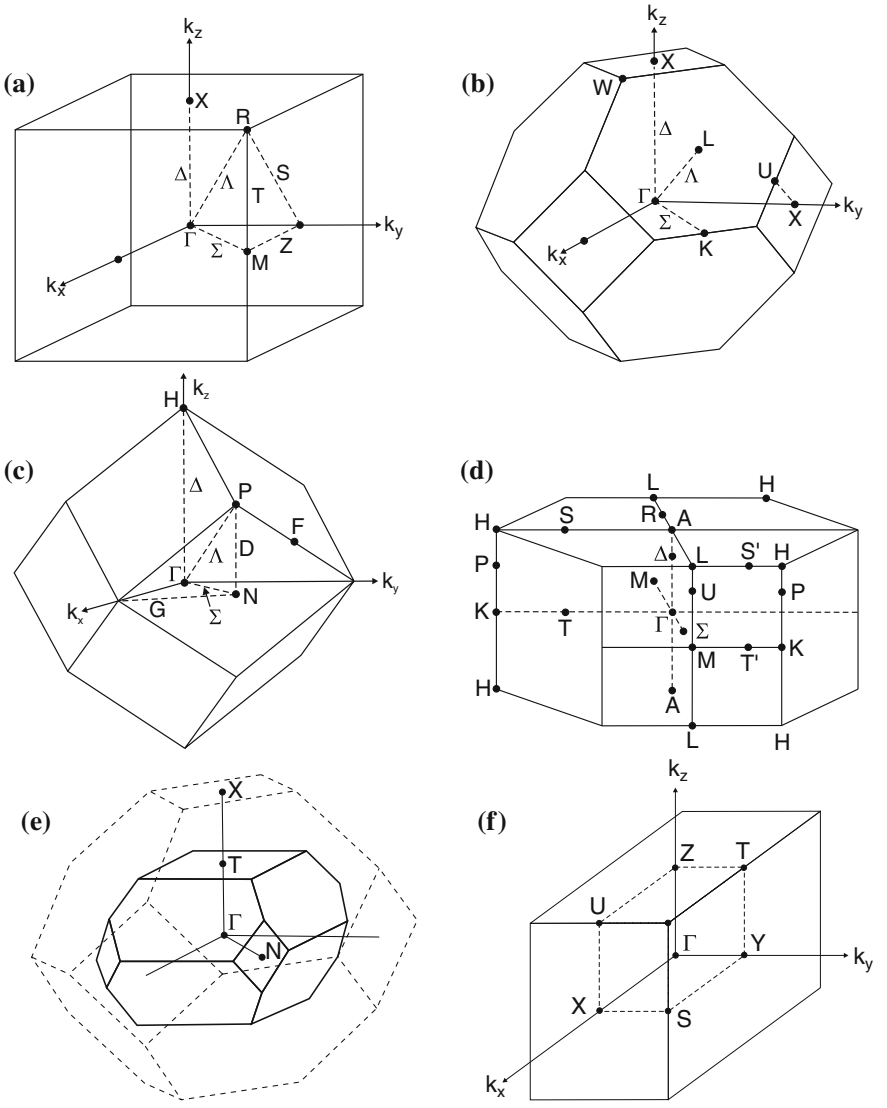

Fig. 3.34 Brillouin zones and special **k** points for the (**a**) primitive cubic (pc), (**b**) fcc, (**c**) bcc, and (**d**) hcp lattice. (**e**) Brillouin zone for chalcopyrite structure with fcc Brillouin zone shown as *dashed outline*. (**f**) Brillouin zone for orthorhombic lattice with one quadrant shown with *dashed lines*.

In the Brillouin zone of the fcc lattice (Si, Ge, GaAs, …) the X point denotes the point at the zone boundary in ⟨001⟩-directions (at distance $2\,\pi/a$ from Γ), K for ⟨110⟩-directions (at distance $3\,\pi/\sqrt{2}\,a$ from Γ) and L for the ⟨111⟩-directions (at distance $\sqrt{3}\,\pi/a$ from Γ) (see Table 3.6). The straight paths from Γ to X, K, and L are denoted as Δ, Σ, and Λ, respectively. High symmetry points and directions of the Brillouin zone of the hcp lattice are given in Table 3.7.

3.7 Alloys

When different semiconductors are mixed various cases can occur:

- The semiconductors are not miscible and have a so-called miscibility gap. They will tend to form clusters that build up the crystal. The formation of defects is probable.
- They form an ordered (periodic) structure that is called a superlattice.
- They form a random alloy.

3.7.1 Random Alloys

Alloys for which the probability to find an atom at a given lattice site is given by the fraction of these atoms (i.e. the stoichiometry), independent of the surrounding, are called *random* alloys. Deviations from the random population of sites is termed *clustering*.

For a Ge_xSi_{1-x} alloy this means that any given atom site has the probability x to have a Ge atom and $1-x$ to have a Si atom. The probability p_n that a Si atom has n next-neighbor Ge atoms is

$$p_n = \binom{4}{n} x^n\,(1-x)^{4-n}, \tag{3.22}$$

and is depicted in Fig. 3.35 as a function of the alloy composition. The symmetry of the Si atom is listed in Table 3.8. If it is surrounded by four of the same atoms (either Ge or Si), the symmetry is T_d. If one atom is different from the other three next neighbors, the symmetry is reduced to C_{3v} since one bond is singled out. For two atoms each the symmetry is lowest (C_{2v}).

In an alloy from binary compound semiconductors such as $Al_xGa_{1-x}As$ the mixing of the Al and Ga metal atoms occurs only on the metal (fcc) sublattice. Each As atom is bonded to four metal atoms. The probability that it is surrounded by n Al atoms is given by (3.22). The local symmetry of the As atom is also given by Table 3.8. For $AlAs_xP_{1-x}$ the mixing occurs on the nonmetal (anion) sublattice. If the alloy contains three atom species it is called a *ternary* alloy. In Fig. 3.36 the $(1\bar{1}0)$ surface

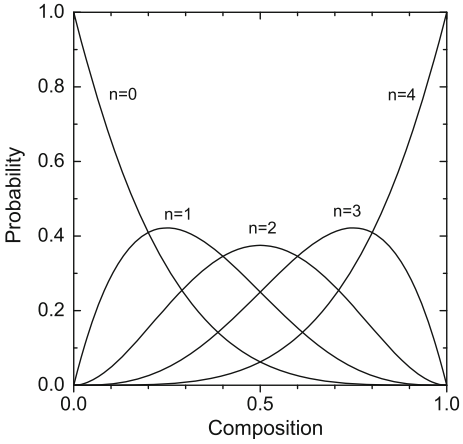

Fig. 3.35 Probability that a Si atom has n next-neighbor Ge atoms in a random Ge_xSi_{1-x} alloy

Table 3.8 Probability p_n (3.22) and symmetry of an A atom being surrounded by n B atoms in a tetrahedrally configured B_xA_{1-x} random alloy

n	p_n	Symmetry
0	x^4	T_d
1	$4\,x^3\,(1-x)$	C_{3v}
2	$6\,x^2\,(1-x)^2$	C_{2v}
3	$4\,x\,(1-x)^3$	C_{3v}
4	$(1-x)^4$	T_d

(UHV cleave) of an $In_{0.05}Ga_{0.95}As$ alloy is shown. Indium atoms in the first layer show up as brighter round dots [214]. Along the [001]-direction the positions are uncorrelated, along [110] an anti-correlation is found, corresponding to an effective repulsive pair interaction energy of 0.1 eV for the nearest neighbor In–In pairs along the [110]-direction due to strain effects [215].

If the binary end components have different crystal structure, the alloy shows a transition (or compositional transition range) from one structure to the other at a particular concentration. An example is the alloy between wurtzite ZnO and rocksalt MgO. $Mg_xZn_{1-x}O$ alloy thin films exhibits wurtzite structure up to about $x = 0.5$ and rocksalt structure for $x > 0.6$ [216] (cmp. Fig. 3.39).

If the alloy contains four atom species it is called *quaternary*. A quaternary zincblende alloy can have the mixing of three atom species on one sublattice, such as $Al_xGa_yIn_{1-x-y}As$ or $GaAs_xP_ySb_{1-x-y}$ or the mixing of two atom species on both of the two sublattices, such as $In_xGa_{1-x}As_yN_{1-y}$.

The random placement of different atoms on the (sub)lattice in an alloy represents a perturbation of the ideal lattice and causes additional scattering (alloy scattering). In the context of cluster formation, the probability of an atom having a direct neighbor of the same kind on its sublattice is important. Given a $A_xB_{1-x}C$ alloy, the probability p_S to find a single A atom surrounded by B atoms is given by (3.23a). The probability

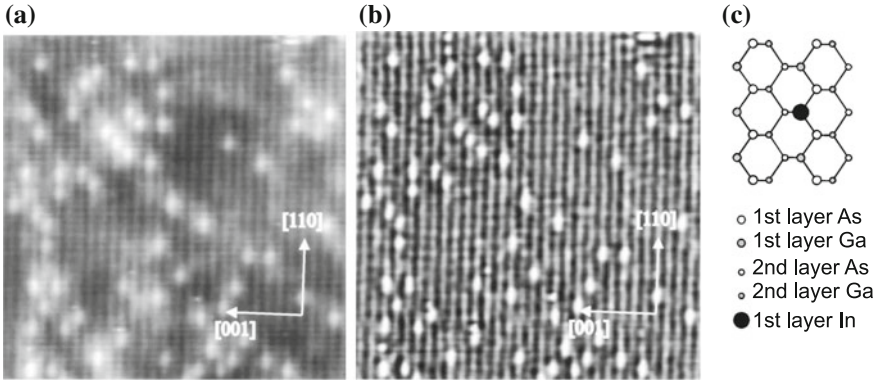

Fig. 3.36 (**a**) STM empty-state image ($17.5 \times 17.5\,\mathrm{nm}^2$) of the $(1\bar{1}0)$ surface of an MBE-grown $In_{0.05}Ga_{0.95}As$ alloy on GaAs, (**b**) curvature-enhanced image. (**c**) Schematic atomic arrangement of the first and second atomic layer. Adapted from [215]

p_{D^1} to find a cluster of two neighbored A atoms surrounded by B atoms is given by (3.23b).

$$p_S = (1-x)^{12} \tag{3.23a}$$

$$p_{D^1} = 12\,x\,(1-x)^{18}. \tag{3.23b}$$

These formulas are valid for fcc and hcp lattices. For larger clusters [217, 218], probabilities in fcc and hcp structures differ.

3.7.2 Phase Diagram

The mixture A_xB_{1-x} with average composition x between two materials A and B can result in a single phase (alloy), a two-phase system (phase separation) or a metastable system. The molar free enthalpy ΔG of the mixed system is approximated by

$$\Delta G = \Omega\,x\,(1-x) + kT\,[x\,\ln(x) + (1-x)\,\ln(1-x)]\,. \tag{3.24}$$

The first term on the right-hand side of (3.24) is the (regular solution) enthalpy of mixing with the interaction parameter Ω, which can depend on x. The second term is the ideal configurational entropy based on a random distribution of the atoms. The function is shown for various ratios of kT/Ω in Fig. 3.37a. In an equilibrium phase diagram (see Fig. 3.37b) the system is above the binodal curve in one phase (miscible). On the binodal line $T_b(x)$ in the (x, T) diagram the A- and B-rich disordered phases have equal chemical potentials, i.e. $\partial G/\partial x = 0$. For Ω independent of x the temperature T_b is given by (3.25a). A critical point is at the maximum temperature

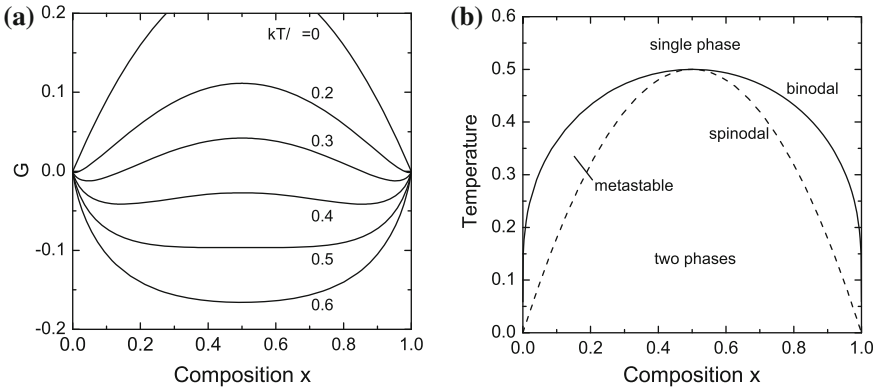

Fig. 3.37 (**a**) Free enthalpy ΔG of mixed binary system (3.24) in units of Ω for $\Omega = \text{const.}$ and various values of kT/Ω as labeled. (**b**) Schematic phase diagram for binary mixture. The temperature is given in units of Ω/k. The *solid* (*dashed*) denotes the binodal (spinodal) line

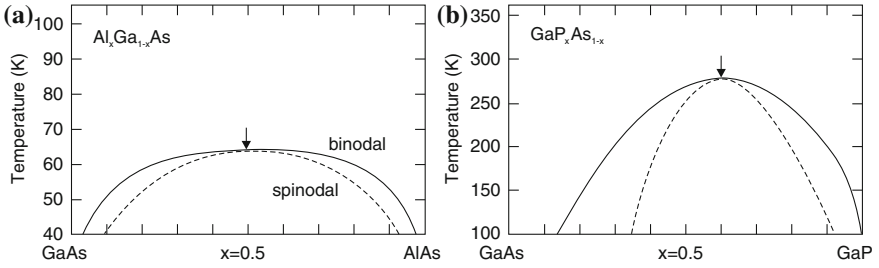

Fig. 3.38 Calculated phase diagrams for (**a**) $Al_xGa_{1-x}As$ and (**b**) GaP_xAs_{1-x}. The binodal (spinodal) curve is shown as *solid* (*dashed*) line. Adapted from [219]

T_{mg} and concentration x_{mg} of the miscibility gap. For Ω independent of x it is given by $T_{\text{mg}} = \Omega/2$ and $x_{\text{mg}} = 1/2$. In the region below the spinodal boundary, the system is immiscible and phases immediately segregate (by spinodal decomposition). On the spinodal line $T_{\text{sp}}(x)$ the condition $\partial^2 G/\partial x^2 = 0$ is fulfilled. For Ω independent of x the temperature T_{sp} is given by (3.25b). The region between the binodal and spinodal curves is the metastable region, i.e. the system is stable to small fluctuations of concentration or temperature but not for larger ones.

$$kT_{\text{b}}(x) = \Omega \frac{2x-1}{\ln(x) - \ln(1-x)} \tag{3.25a}$$

$$kT_{\text{sp}}(x) = 2\Omega\, x\,(1-x). \tag{3.25b}$$

In Fig. 3.38 calculated diagrams for GaAs-AlAs and GaAs-GaP [219] are shown. The arrows denote the critical point. These parameters and the interaction parameters for a number of ternary alloys are given in Table 3.9. For example, for $Al_xGa_{1-x}As$

Table 3.9 Calculated interaction parameter $\Omega(x)$ (at $T = 800\,\mathrm{K}$, 1 kcal/mol= 43.39 meV), miscibility-gap temperature T_{mg} and concentration x_{mg} for various ternary alloys

Alloy	T_{mg} (K)	x_{mg}	$\Omega(0)$ (kcal/mol)	$\Omega(0.5)$ (kcal/mol)	$\Omega(1)$ (kcal/mol)
$Al_xGa_{1-x}As$	64	0.51	0.30	0.30	0.30
GaP_xAs_{1-x}	277	0.603	0.53	0.86	1.07
$Ga_xIn_{1-x}P$	961	0.676	2.92	3.07	4.60
$GaSb_xAs_{1-x}$	1080	0.405	4.51	3.96	3.78
$Hg_xCd_{1-x}Te$	84	0.40	0.45	0.80	0.31
$Zn_xHg_{1-x}Te$	455	0.56	2.13	1.88	2.15
$Zn_xCd_{1-x}As$	605	0.623	2.24	2.29	2.87
$In_xGa_{1-x}N$	1505	0.50	6.32	5.98	5.63

Data for (In,Ga)N from [220], other data from [219]

complete miscibility is possible for typical growth temperatures (>700 K), but for $In_xGa_{1-x}N$ the In solubility at a typical growth temperature of 1100 K is only 6 % [220].

The alloy system (Al,Ga,In)(As,P,Sb) always crystallizes in the zincblende structure and (Al,Ga,In)N always in the wurtzite structure. If the binary end components of a ternary alloy have a *different* crystal structure things become more complicated and the crystal phase has to be determined experimentally (and modelled) for each composition. As an example the energy of the wurtzite, hexagonal and rocksalt structure of $Mg_xZn_{1-x}O$ has been calculated [221] as depicted in Fig. 3.39 (cmp. Fig. 2.4 for silicon). The transition between wurtzite and rocksalt structure is predicted for $x = 0.33$.

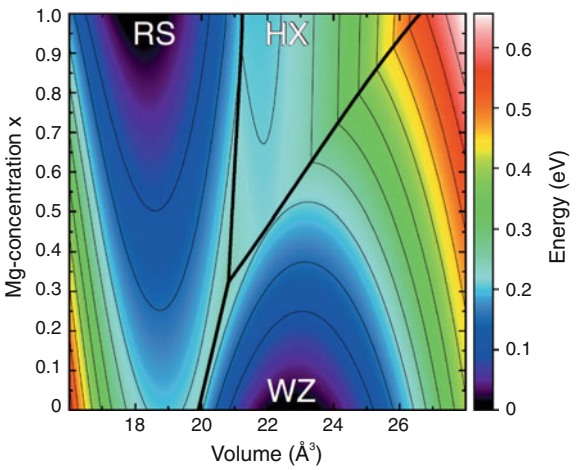

Fig. 3.39 Calculated energy versus volume of the formula unit for $Mg_xZn_{1-x}O$ in the wurtzite (WZ), hexagonal (HX) and rocksalt phase (RS). The separations between the three phase are denoted by *straight bold lines*. Adapted from [221]

3.7.3 Virtual Crystal Approximation

In the *virtual crystal approximation* (VCA) the disordered alloy AB_xC_{1-x} is replaced by an ordered binary compound AD with D being a 'pseudoatom' with properties that are configuration averaged over the properties of the B and C atoms, e.g., their masses or charges. Such an average is weighted with the ternary composition, e.g., the mass is $M_D = xM_B + (1-x)M_C$. For example, the A–D force constant would be taken as the weighted average over the A–B and A–C force constants.

3.7.4 Lattice Parameter

In the VCA for an alloy a new sort of effective atom is assumed that has an averaged bond length that depends linearly on the composition. Typically, Vegard's law (3.26), which predicts that the lattice constant of a ternary alloy $A_xB_{1-x}C$ depends linearly on the lattice constants of the binary alloys AC and BC, is indeed fulfilled

$$a_0(A_xB_{1-x}C) = a_0(BC) + x\,[a_0(AC) - a_0(BC)]. \tag{3.26}$$

In reality, the bond length of the AC and BC bonds changes rather little (Fig. 3.40a) such that the atoms in the alloy suffer a displacement from their average position and the lattice is deformed on the nanoscopic scale. In a lattice of the type $In_xGa_{1-x}As$ the anions suffer the largest displacement since their position adjusts to the local cation environment. For $In_xGa_{1-x}As$ a bimodal distribution, according to the As–Ga–As and As–In–As configurations, is observed (Fig. 3.40b). The cation–cation second-neighbor distances are fairly close to the VCA.

While the average lattice parameter in alloys changes linearly with composition, the cell-internal parameter u (for wurtzite structures, see Sect. 3.4.5) exhibits a nonlinear behavior as shown in Fig. 3.41. Therefore physical properties connected to u, such as the spontaneous polarization, will exhibit a bowing.

3.7.5 Ordering

Some alloys have the tendency for the formation of a superstructure [225]. Growth kinetics at the surface can lead to specific adatom incorporation leading to ordering. For example, in $In_{0.5}Ga_{0.5}P$ the In and Ga atoms can be ordered in subsequent (111) planes (CuPt structure) instead of being randomly mixed (Fig. 3.42). This impacts fundamental properties such as the phonon spectrum or the band gap. CuPt ordering on (111) and $(\bar{1}\bar{1}1)$ planes is called $CuPt_A$, on $(\bar{1}11)$ and $(1\bar{1}1)$ planes $CuPt_B$ ordering. In Fig. 3.43, a TEM image of a $Cd_{0.68}Zn_{0.32}Te$ epilayer is shown with simultaneous

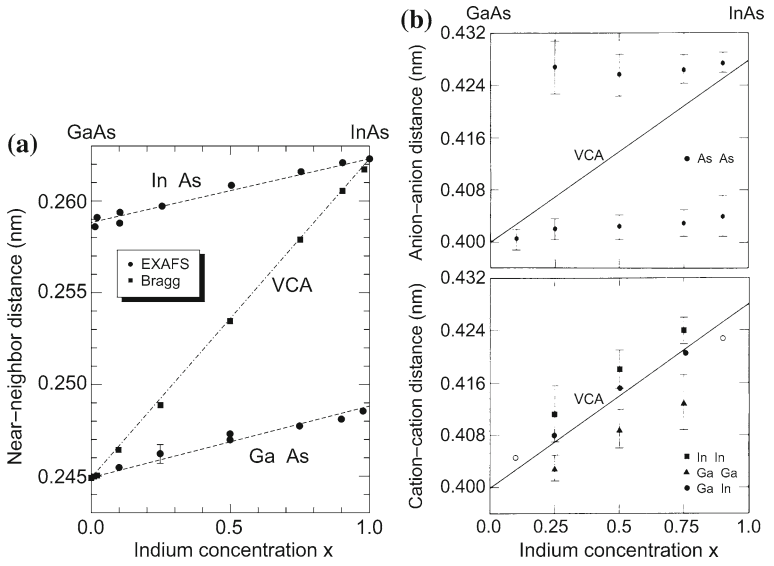

Fig. 3.40 (**a**) Near-neighbor distance ($\sqrt{3}\,a_0/4$) of $In_xGa_{1-x}As$ as measured by standard X-ray diffraction (Bragg reflection, *solid squares*) and VCA approximation (*dash-dotted line*). Near-neighbor Ga–As and In–As distances as determined by EXAFS (extended X-ray absorption fine structure, *solid squares*). *Dashed lines* are guides to the eye. Data from [222]. (**b**) Second-neighbor distances for $In_xGa_{1-x}As$ as determined from EXAFS, *top*: anion–anion distance (for As–As), *bottom*: cation–cation distance (for In–In, Ga–Ga, and Ga–In). *Solid lines* in both plots are the VCA ($a_0/\sqrt{2}$). Data from [223]

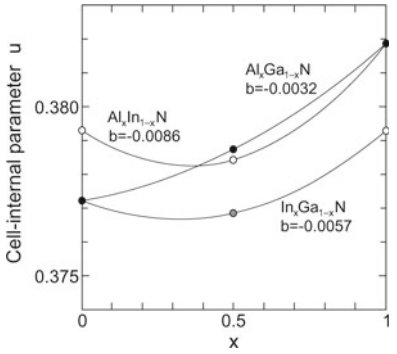

Fig. 3.41 Theoretical values ($T = 0\,\mathrm{K}$) for the cell-internal parameter u as a function of the composition for group-III nitride alloys. The *solid lines* are quadratic curves (bowing parameter b is shown) through the points for $x = 0$, 0.5, and 1.0. Data from [224]

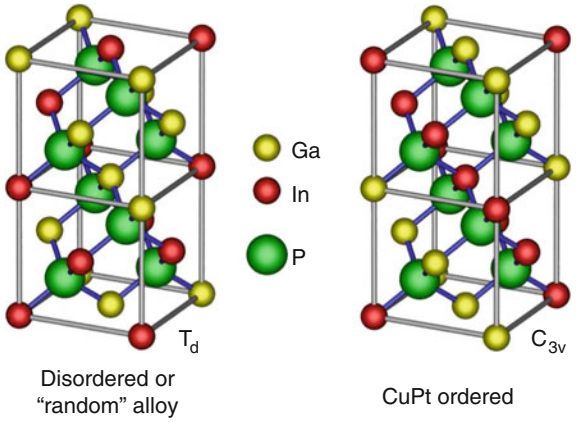

Fig. 3.42 CuPt-ordered ternary alloy $In_{0.5}Ga_{0.5}P$; the lattice symmetry is reduced from T_d to C_{3v}

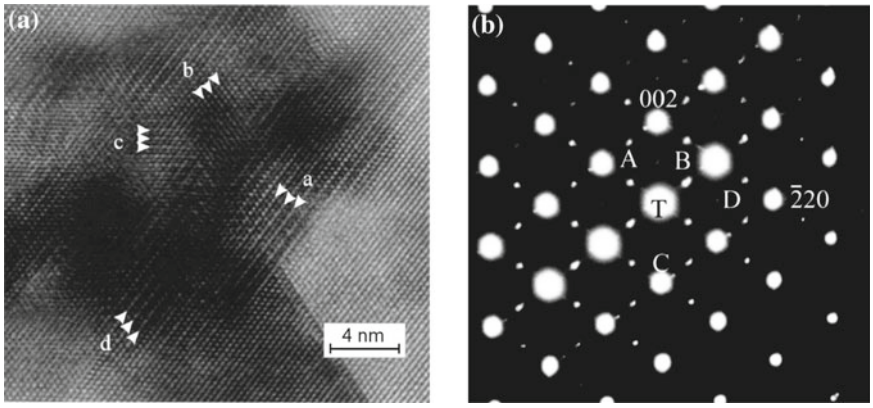

Fig. 3.43 (**a**) Cross-sectional transmission electron microscope image along the [110] zone axis of a $Cd_{0.68}Zn_{0.32}Te$ epilayer on GaAs showing ordered domains having a doublet periodicity on the {111} and {001} lattice planes. Two different {111} variants are labeled 'a' and 'b'. The doublet periodicity in the [001] is seen in the 'c' region. (**b**) Selected-area diffraction pattern along the [110] zone. Strong peaks are fundamental peaks of the zincblende crystal, weak peaks are due to CuPt ordering, labeled A and B, and CuAu-I ordering, labeled C and D. The latter are the weakest due to a small volume fraction of CuAu-ordered domains. Adapted from [226]

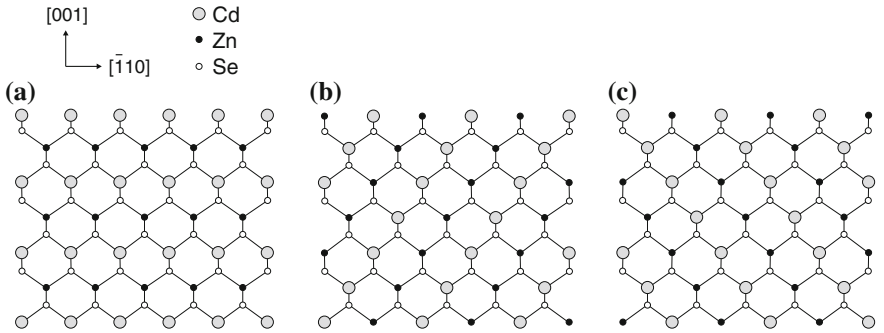

Fig. 3.44 Schematic diagrams of zincblende $Cd_xZn_{1-x}Te$ along [110] with (**a**) CuAu-I type ordering and (**b**,**c**) two types of the $CuPt_B$ type ordering. Doublet periodicity is along (**a**) [001] and [$\bar{1}$10], (**b**) [1$\bar{1}$1] and (**c**) [$\bar{1}$11]. Adapted from [226]

ordering in the CuPt structure (doublet periodicity along $\left[1\bar{1}1\right]$ and $\left[\bar{1}11\right]$) and in the CuAu-I structure[6] (doublet periodicity along [001] and [$\bar{1}$10]) (Fig. 3.44).

[6]The CuAu-I structure has tetragonal symmetry. There exists also the CuAu-II structure that is orthorhombic.